Temporally resolved kinase regulatory networks control endothelial barrier integrity

Ling Wei,[1] Selasi Dankwa,[1] Kamalakannan Vijayan,[1] Joseph D. Smith,[1,2,3,*] and Alexis Kaushansky[1,2,3,4,*]

[1]Center for Global Infectious Disease Research, Seattle Children's Research Institute, Seattle, WA 98109, USA

[2]Department of Pediatrics, University of Washington, Seattle, WA 98105, USA

[3]Department of Global Health, University of Washington, Seattle, WA 98105, USA

[4]Lead contact

*Correspondence: alexis.kaushansky@seattlechildrens.org (A.K.), joseph.smith@seattlechildrens.org (J.D.S.)

SUMMARY

Breakdown of the blood-brain barrier is triggered by a range of physiological and pathological stimuli and is detrimental for brain function. Yet, the underlying signaling networks regulating barrier integrity are incompletely understood. Here, we present a novel and generalizable tool, Temporally REsolved KInase Network Generation (TREKING), that combines machine learning and network reconstruction to build time-resolved, functional phosphosignaling networks. We investigated kinase-driven pathways that modulate barrier permeability in brain endothelial cells in the presence of inflammatory stimuli. Our results reveal that >100 kinases are functional during barrier insult and provide time-resolved molecular insights into the differential networks that drive barrier disruption and recovery. The resulting models suggest a multi-layered rewiring of thrombin-induced barrier disruption following TNFα priming, including the timing of common signaling pathways, condition-specific phosphosignaling networks, and a skewing at major signaling hubs towards barrier-weakening activities. TREKING provides a novel tool for dissecting temporal phosphosignaling networks in biological systems.

Keywords: Endothelial barrier permeability, thrombin, TNFα, kinase regression, self-organizing map, phosphosignaling network

INTRODUCTION

Homeostasis of the central nervous system (CNS) is tightly regulated by the blood-brain barrier (BBB). Dysregulation of the BBB can cause ions, neurotoxic plasma components, pathogens and immune cells to enter the CNS, which leads to massive disruption and degeneration (Daneman and Prat, 2015). BBB derangements are associated with the pathogenesis of a variety of diseases, including infectious causes such as cerebral malaria and non-infectious causes such as multifactorial neurodegenerative diseases (Miller et al., 2013; Zhao et al., 2015).

The permeability of endothelial barriers is tightly regulated via cell-cell junctions and focal adhesions. These points of cell-cell and cell-substrate contact are controlled by contractile mechanisms, whose functions are heavily regulated by phosphosignaling (Mehta and Malik, 2006). Kinases, via phosphorylation, can rapidly (on the scale of seconds to minutes) alter cellular states in response to barrier-disruptive stimuli and can promote long-term regulatory functions during barrier recovery (Kuppers et al., 2014). Whereas kinases that mediate barrier function have been intensively explored, work to date has largely focused on characterizing specific molecular mediators of barrier perturbation, without evaluating their complex network-level connectivity with other functional modules (Dankwa et al., 2021; Komarova et al., 2017; Kuppers et al., 2014; Mehta and Malik, 2006). Moreover, there is limited understanding of the phosphosignaling pathways involved in restoration of barrier integrity. Understanding the temporal dynamics of barrier regulation is critical for designing successful targeted therapeutic interventions.

During infection or disease, endothelial cells must integrate complex inflammatory signals. For instance, both thrombin, a multi-functional enzyme, and TNFα, an inflammatory cytokine, can promote morphological remodeling of the endothelium that leads to the loss of barrier integrity (Marcos-Ramiro et al., 2014; Oldenburg and de Rooij, 2014). TNFα exacerbates thrombin-induced barrier disruption (Anrather et al., 1997; Liu et al., 2004; Tiruppathi et al.,

2001), which strongly indicates that endothelial signaling pathways and/or their kinetics are altered by combined inflammatory stimuli. High-resolution and time-resolved phosphoproteomic analyses have cataloged phosphorylation events that occur in response to thrombin or TNFα-induced endothelial activation (Beguin et al., 2019; van den Biggelaar et al., 2014). Separate efforts have developed computational tools and modeling approaches that use -omics data for network generation, including logic modeling such as Boolean logic models and logic ordinary differential equations (ODEs), and enrichment-based approaches such as kinase-substrate enrichment analysis (KSEA) (Casado et al., 2013; Schafer et al., 2019; Vaga et al., 2014). However, these computational tools typically rely on large-scale phosphoproteomics data that can typically not be collected with fine temporal resolution. Furthermore, proteomics only indirectly assesses kinase functionality, as inferred by phosphorylation states. Given these limitations, existing network-generation tools have not yet been applied to elucidating the time-resolved molecular functional underpinnings of endothelial barrier integrity.

Kinase regression (KiR) combines a chemical screen with elastic net regression to broadly interrogate the function of hundreds of kinases in a cellular phenotype (Arang et al., 2017; Dankwa et al., 2021; Gujral et al., 2014). We have previously shown that kinase inhibitors have dramatically different effects on endothelial barrier permeability and their effects exhibit temporal features in barrier disruption and barrier recovery phases (Dankwa et al., 2021), suggesting that different sets of kinase regulators are functional at different stages of barrier perturbation. Here, we develop a novel approach, Temporally REsolved KInase Network Generation (TREKING), to investigate phosphosignaling in disrupted endothelial monolayers induced by thrombin in the presence or absence of TNFα pre-conditioning. TREKING allows 1) assessment of time-resolved kinase functionality associated with barrier regulation, 2) construction of phenotype-driving kinase-mediated phosphosignaling networks that recapitulate signaling events at different stages of barrier perturbation, and 3) systematic comparison of

phosphosignaling between conditions. Our results reveal commonalities and divergences of kinase signaling in response to classic pro-inflammatory stimuli, and insight into signaling pathways with barrier-weakening or barrier-strengthening activity. This novel approach is easily generalizable to other biological systems and will be particularly useful in deconvolving condition-specific, temporally resolved signaling mechanisms important for many phenotypes of interest.

RESULTS

TNFα pre-conditioning alters kinase determinants of thrombin-induced barrier perturbations

In monolayers of human brain microvascular endothelial cells (HBMECs), TNFα pre-conditioning exacerbated thrombin-induced barrier disruption, as demonstrated by the increased maximum barrier permeability and prolonged barrier recovery (Fig. 1A). While this finding is consistent with previous reports (Tiruppathi et al., 2001), the molecular networks that regulate these differences remain unknown.

Here, we introduce TREKING, a generalizable methodology that leverages temporal KiR to build time-resolved networks of kinase signaling from temporal datasets (Fig. S1). First, to identify kinases involved in barrier integrity, a KiR screen was conducted with 28 kinase inhibitors for their impact on barrier permeability in monolayers of HBMECs treated with thrombin (-/+TNFα pre-conditioning) (Dankwa et al., 2021). Kinase inhibitors were added six minutes after thrombin treatment and barrier permeability was assessed in real time using xCELLigence. Different kinase inhibitors blunt, have minimal effect, or exacerbate thrombin-induced barrier disruption and exhibit temporal features during the 6-hour time window (Fig. 1B) (Dankwa et al., 2021).

We reasoned that if identical kinases control the barrier integrity in the two inflammatory conditions, we expect perfect correlation between the activities of the 28 kinase inhibitors in thrombin alone and TNFα pre-conditioned settings. If entirely different kinases control the barrier integrity in the two conditions, we would expect little correlation between the activities of the kinase inhibitors. Thus, the correlation between kinase inhibitor activities serves as an indirect assessment of the similarity of the underlying barrier regulatory phosphosignaling networks across conditions. Using area under the curve (AUC) of the normalized cell index as the metric, we compared the barrier permeability between +thrombin and TNFα pre-conditioning +thrombin conditions across the following time windows: maximum barrier disruption (0-10 minutes), early barrier recovery (25-35 minutes), late barrier recovery (115-125 minutes for +thrombin condition, 235-245 minutes for TNFα pre-conditioning +thrombin condition). The correlation was the lowest within the first ten minutes of kinase inhibitor treatment (Pearson's r = 0.72) and increased during early barrier recovery (Pearson's r = 0.90 to 0.91) (Fig. 1C-D). This suggests that phosphosignaling networks are more divergent during barrier disruption, whereas more similar phosphosignaling networks regulate barrier restoration. The correlation reduced in the late barrier recovery phase (Pearson's r = 0.85 to 0.77) (Fig. 1C-D), perhaps suggesting that a subset of different kinase networks regulate the transition to barrier homeostasis after injury. This analysis is consistent with a model that TNFα pre-conditioning alters kinase regulatory networks that dictate the extent and kinetics of thrombin-induced barrier disruption and recovery in brain endothelial cells.

Time-resolved predictions of barrier-weakening and barrier-strengthening kinases between the two inflammatory conditions

Previously, we predicted 29 and 25 kinases that regulate the HBMEC barrier in response to thrombin treatment with or without TNFα pre-conditioning, respectively. Fifteen kinases were shared between the two conditions (Dankwa et al., 2021). However, these KiR predictions were

based on the full AUC (6-hour time window, post-thrombin treatment), and did not take into account when a kinase was functionally active (i.e., a “functional window”). To address this lack of temporal resolution, we performed a temporal KiR (tKiR), using a sliding window analysis; a 5-minute sliding time window was applied to the normalized cell index data, which slides at 1-minute steps for the first two hours after kinase inhibitor treatment and at 5-minute steps afterwards (Fig. 2A). Among the 300 protein kinases used for tKiR (STAR Methods), the number of functional kinases increased to 120 and 108 in HBMECs treated with thrombin -/+TNFα pre-conditioning, respectively (Fig. 2A, Table S1). The higher resolution of tKiR is because the sliding window analysis allows for the detection of kinases whose activity is brief or sporadic. In total, 159 kinases (~30% of the human kinome) were predicted to regulate barrier function within the 6-hour timeframe, with 69 kinases being common to the two conditions (Fig. 2A).

As a further refinement, the elastic net models were used to predict the direction of barrier activity (weakening or strengthening) in a time-resolved manner (Fig. 2B-C, Fig. S1). For HBMECs not pre-conditioned with TNFα, 53 and 60 kinases were predicted to play a barrier-weakening and barrier-strengthening roles, respectively (Fig. 2B). In addition, seven kinases were predicted to play both barrier-weakening and barrier-strengthening roles during different time windows; we termed these “switch kinases” (Fig. 2B). For HBMECs pre-conditioned with TNFα, 58 and 47 kinases were predicted respectively to be barrier-weakening and barrier-strengthening, and 3 switch kinases were predicted (Fig. 2C). Overall, a greater number of barrier-weakening kinases were predicted early during the time course, whereas barrier-strengthening kinases were predominant during late barrier recovery and plateau phases (Fig. 2D). Nevertheless, multiple barrier-strengthening kinases were identified at the earliest time windows following thrombin treatment, indicating that cells propagate both types of barrier activities concurrently (Fig. 2D).

The tKiR predictions of kinase activity recapitulate the canonical signaling pathways involved in barrier regulation

Assessing position of predicted kinases within canonical signaling pathways is one way to evaluate the integrity of tKiR. For instance, if kinase A phosphorylates kinase B, we would expect kinase A to be active at earlier time points than kinase B. Previous work has established that mitogen-activated protein kinase (MAPK) cascades are involved in thrombin signaling, including the extracellular signal-regulated kinases (ERKs), Jun N-terminal kinases (JNKs) and p38 MAPKs (Mehta and Malik, 2006; Minami et al., 2004; Radeva and Waschke, 2018). The topology of MAPKs is well-established; cell surface receptors such as receptor tyrosine kinases (RTKs) provide a link between extracellular stimuli and the cascade (Morrison, 2012). After activation, most MAPK pathways have a four-tier kinase architecture (MAP3K-MAP2K-MAPK-MAPKAPK) (Pimienta and Pascual, 2007). Given the strict directionality of the network, we reasoned that RTKs would be predicted to regulate the barrier during the earliest time points after thrombin treatment, followed sequentially by MAP3Ks, MAP2Ks, MAPKs and then MAPKAPKs.

The ERK, JNK, and p38 pathways were all implicated in thrombin signaling, with multiple kinases in each signaling cascade predicted by tKiR (Fig. 3). The predicted kinases could be assembled into pathways that were consistent with known information flow through the MAPK cascade. Overall, the ERK and JNK pathways were associated with barrier-weakening activity and the p38 pathway had a mixture of barrier-weakening and barrier-strengthening activities mediated by different p38 family members (Fig. 3). For example, within the ERK pathway, all the predicted kinases were barrier-weakening, and their activity profiles followed the expected order of MAP2Ks preceding MAPKs, which preceded four downstream MAPKAPKs (Fig. 3). Likewise, a mid-to-late acting barrier-strengthening p38 pathway could be assembled from known components (Fig. 3).

The same MAPK pathways were predicted with TNFα pre-conditioning (Fig. 3). However, the timing and duration of the ERK and JNK pathways were shifted earlier and shortened for most kinases. We also observed a second wave of barrier-weakening activity by MAPK1/ERK2, and multiple additional kinases in the JNK pathway were predicted, consistent with previous work indicating that combined TNFα and thrombin treatment alters the magnitude and duration of JNK phosphorylation activation marks in endothelial cells (Liu et al., 2004). Furthermore, the p38 pathway became nearly entirely barrier-strengthening with TNFα pre-conditioning and MAPKAPK2/MK2 was no longer predicted to be a switch kinase with dual barrier-weakening and barrier-strengthening activities. Consequently, this analysis suggests that core MAPK signaling pathways involved in thrombin-induced barrier disruption remain intact after TNFα pre-conditioning, but the timing, duration, and importance of specific MAPKs are altered.

To experimentally assess the model, we evaluated kinase phosphorylation of a subset of tKiR predicted kinases in ERK, JNK and p38 pathways via western blot. HBMECs (-/+TNFα pre-conditioning) were treated with thrombin for 0, 5, 15, 30, 60, 120, 180, 240 or 360 minutes. In each experimental condition, the level of phosphorylated kinase after thrombin treatment was compared to its phosphorylation at basal level (media only). By western blot, increased levels of activated kinases were detected in each of the three MAPK pathways at different time frames during barrier disruption and barrier recovery (Fig. 4A). In both +thrombin and TNFα pre-conditioning +thrombin conditions the activity of MAP2K1/2 (MEK1/2) peaked at an earlier time point compared to its downstream targets MAPK1/ERK2 and MAPK3/ERK1, which supports the tKiR model predictions of early barrier-weakening functionality of these MAPKs (Fig. 4A). Results from western blot also showed that the activity of MAPK9/JNK2 increased upon thrombin treatment and remained higher than the basal level six hours after thrombin treatment, at which point the barriers were mostly recovered (Fig. 4A). Similarly, the activity of p38 MAPKs

was increased shortly after thrombin treatment, and in both +thrombin and TNFα pre-conditioning +thrombin conditions an early (barrier disruption phase) and a late (late barrier recovery phase) activity peak were detected. Overall, in most cases there was increasing phosphorylation immediately preceding or overlapping corresponding time windows of predicted barrier activity for all three canonical MAPK pathways (Fig. 4B).

Construction of phosphosignaling networks that mediate barrier disruption

To investigate how endothelial cells propagate phosphosignals to and from key kinase regulators beyond canonical linear cascades, we reconstructed kinase phosphosignaling networks by first using self-organizing maps (SOMs), a dimensionality reduction method that can capture the topographic relationships of time series data (Kohonen, 1982). Kinases of similar temporal functionality were clustered into one neuron, and neurons having similar mean temporal functionality are more closely located on the SOM (Fig. 5A, Fig. S2A-C). To generate the SOMs, we used a grid size of 6×6 (resulting in a maximum of 36 neurons). In +thrombin condition, we obtained 30 neurons and each neuron contained between 1 and 11 kinases (Fig. 5A, Fig. S2D, Table S2). After TNFα-preconditioning, we obtained 35 neurons and each neuron contained between 1 and 9 kinases (Fig. S2A, D, Table S2).

Since kinases assigned to the same neuron exhibit similar temporal barrier functionality, we reasoned that they are more likely to act within a connected signaling module. To build phosphosignaling pathways and investigate systems-level interconnections, we built TREKING models of barrier phosphosignaling networks (Fig. S1, Fig. S2E). For each neuron a local phosphosignaling network was built to describe the paths through which phosphosignals may propagate, using the kinase-substrate phosphorylation database PhosphoSitePlus® to predict upstream and downstream kinases and to infer intermediate kinases in the pathways (Fig. S2E) (Hornbeck et al., 2015). We were able to build 26 local networks from the 30 neurons generated in +thrombin condition, and 27 local networks from the 35 neurons generated in TNFα pre-

conditioning +thrombin condition (Table S2). The remaining neurons included only a single kinase that does not self-phosphorylate or multiple unconnected kinases. The size and topology of the phosphosignaling networks varied across neurons. In +thrombin condition, most networks have a maximum node-to-node shortest path length below 10 kinases, while the deepest networks built from neurons (0,0) and (3,3) have a maximum shortest path length of 14 kinases (Fig. S2E). In TNFα pre-conditioning +thrombin condition, most networks have a maximum shortest path length ranging from 3 to 9 kinases, except for the network built from neuron (2,4) that has a maximum shortest path length of 16 kinases (Fig. S2E).

The SOM analysis revealed substantial interconnections between MAPK and NF-κB signaling pathways in both barrier-weakening and barrier-strengthening activities. For instance, in +thrombin condition, the barrier-weakening neurons (0,0) and (1,0) include a mixture of ERK, JNK, and canonical NF-κB signaling pathways with MAPK3/ERK1, CHUK/IKKα and MAPKAPK3/MK3 in neuron (0,0) and MAPK1/ERK2 and MAPK8/JNK1 in neuron (1,0) (Fig 5A-B, Table S2). Likewise, a mid-to-late barrier-strengthening neuron (5,5) contained the switch kinase MAPKAPK2/MK2 in a p38 pathway (MAP3K20/ZAK-MAPK14/p38α-MAPKAPK2/MK2), CSK (C-terminal Src kinase; a negative regulator of Src-family kinases (SFKs)), and two members of non-canonical NF-κB signaling pathways (MAP3K14/NIK and IKBKB/IKKβ) (Fig. 5C-D). Therefore, MAPK and NF-κB interconnections were implicated in both barrier disruption and barrier recovery phases. Notably, with TNFα pre-conditioning, this barrier-strengthening pathway shrunk to MAP3K20/ZAK-MAPK14/p38α (p38 pathway) and MAP3K14/NIK (NFκB signaling pathway). Overall, 77 of the 120 predicted kinases in +thrombin condition and 61 of the 108 predicted kinases in TNFα pre-conditioning +thrombin condition could be assembled by TREKING into signaling pathways of two or more kinases that acted with similar temporal kinetics and identified potential network-level interconnections between individual barrier signaling pathways within the broader signaling networks.

TNFα pre-conditioning alters the landscape of kinase regulators and associated pathways in the barrier disruption and barrier recovery phases

To further investigate the phosphosignaling networks associated with thrombin-induced barrier perturbation, and how these networks were altered in response to TNFα pre-conditioning, we decided to investigate barrier disruption and barrier recovery phases separately. To investigate networks that led to barrier disruption, we first built the composite phosphosignaling networks important for barrier regulation during the barrier disruption phase (Fig. S6, Fig. S7). Specifically, networks built from neurons that were functional within the first 30 minutes after thrombin treatment (-/+TNFα) were combined to form a composite network that illustrates the connections between functional kinases in the barrier disruption phase. Interestingly, the composite networks reveal overlapping kinase nodes within barrier-weakening and barrier-strengthening pathways, illustrating nexuses where specific kinases have the capacity to lead to both phenotypes (Fig. S6, Fig. S7).

In the first 30 minutes after thrombin treatment, more kinases were predicted to be barrier-weakening in TNFα pre-conditioning +thrombin condition (40 kinases) than in +thrombin condition (33 kinases), and eighteen barrier-weakening kinases were shared, including multiple members of the MAPK family (Fig. S3A). Among the twenty-two kinases uniquely predicted in TNFα pre-conditioning +thrombin condition were all three members of the Janus kinase (JAK) family (JAK1, JAK2 and JAK3) (Fig. S3A), which are known to be activated by TNFα (Guo et al., 2016).

At the network level, pre-conditioning with TNFα led to a multi-layered rewiring of phosphosignaling including a larger fraction of barrier-weakening signaling pathways, which is manifested both as more barrier-weakening kinase regulators (Fig. S3A) and more barrier-weakening kinase connections (Fig. S6, Fig. S7) in the barrier disruption phase. For instance, the connectivity (in/out-degrees of freedom) of kinase nodes is skewed towards barrier-

weakening connections with TNFα pre-conditioning (Fig. S3B). Moreover, the ratio of barrier signaling activities shifted at major signaling hubs. For example, AKT1 is the most highly connected kinase in the composite networks. Whereas a mixture of signals flow through AKT1 under both inflammatory conditions, barrier-weakening connections predominate with TNFα pre-conditioning (Fig. S3C). This suggests that connectivity of AKT1 is rewired to associate with factors that promote barrier disruption when cells are pre-conditioned with TNFα. Similarly, MAPK1 is balanced between barrier-weakening and barrier-strengthening connections when thrombin is treated alone but skewed towards barrier-weakening connections in the context of TNFα pretreatment (Fig. S6, Fig. S7). Thus, TREKING describes network-level mechanisms by which barrier-weakening activities might be favored after TNFα pre-conditioning.

In addition to repurposing the phosphosignaling network towards barrier-weakening activities in the barrier disruption phase, TNFα priming also altered the network during the barrier recovery phase (Fig. 1). We reasoned that barrier-strengthening signaling activities may begin prior to the repair phase, so we constructed composite networks for the full 6-hour time course (Fig. S8, Fig. S9). At the network level, pre-conditioning with TNFα led to a reduction in the fraction of barrier-strengthening pathways over the entire 6-hour time course. There were several notable differences between the barrier-strengthening networks that might describe the delayed recovery in the presence of TNFα. In the absence of TNFα, networks involving megakaryocyte-associated tyrosine kinase (MATK/CTK) and CSK, both negative regulators of SFKs, are engaged (Fig. S8). During early barrier recovery, the MATK pathway (EPHA1-MATK/CTK-ABL1-FYN-PDGFRA-ARAF) was predicted to be functional, then later the CSK pathway (CSK-MAPK14/p38α-MAPKAPK2/MK2) was predicted to drive barrier recovery (Fig. 5D, Fig. S8). Together, these pathways were predicted to be functional throughout barrier recovery and drive a robust and sustained repair in the absence of TNFα pre-conditioning. In contrast, when cells are pre-conditioned with TNFα, the activity of the CSK pathway is lost (Fig.

S9), providing one hypothesis of why the kinetics of late barrier recovery is distinct after TNFα pre-conditioning. Taken together, this analysis suggests that TNFα pre-conditioning both enhances the number of barrier-weakening networks and rewires barrier-strengthening regulators to alter the magnitude and duration of barrier disruption.

TREKING predicts barrier-specific kinase functionality with temporal resolution

The TREKING model (Fig. S1) predicts activity windows for kinases and the networks through which phosphosignals propagate with temporal resolution. To systematically evaluate the accuracy of the networks predicted to underlie the barrier functionality in response to thrombin, we first used the TREKING model to generate time-resolved predictions of the activation states of kinases in response to thrombin (-/+TNFα pre-conditioning). By considering all the signaling connections that a kinase is associated with, we can comprehensively explore its role in barrier regulation over time. To assess the barrier function of a kinase at a particular time point, a 10-minute time window centered at that time point was applied (Fig. S5A). If any of the signaling pathways that the kinase is associated with are active within the time window, the model predicts the kinase to be functionally active within that time window; otherwise, the model predicts the kinase to be functionally inactive within the time window (Fig. S5A).

To evaluate the accuracy of the TREKING model for predicting kinase activity, we treated HBMECs with thrombin in the presence or absence of TNFα pre-conditioning. We collected cellular lysates at nine time points and evaluated activation of the 14 kinases using western blot (Table S3). TREKING predicted 78 instances of active barrier function across all time points in the absence of TNFα; 61 differential phosphorylation events were observed by western blot (Fig. 6A, Fig. S5B). TREKING predicted 71 instances of active barrier function across all time points after thrombin treatment with TNFα pre-conditioning; we detected 47 differential phosphorylation events by western blot (Fig. 6A, Fig. S5B). These data suggest that TREKING outperforms random models (STAR Methods, Fig. 6B, Fig. S5C-D). TREKING

highlights many examples of altered kinase functionality after TNFα pre-conditioning (Fig. 6A, Fig. S4). For instance, PTK2/FAK was predicted to have sustained activity in the absence of, but not in the presence of TNFα pre-conditioning. PTK2/FAK also exhibits reduced connectivity after TNFα pre-conditioning (Fig. 6A, Fig. S4). The western blot data were consistent with the model predictions that without TNFα pre-conditioning the activity of PTK2/FAK was different from non-treated HBMECs at all time points assessed, while in TNFα pre-conditioned cells a significant reduction in phosphorylation was detected only in the barrier disruption phase (Fig. 6A, Fig. S4).

For highly connected kinases, such as SRC, p38 MAPK, PDPK1, and AKT1, TREKING predicted that upon thrombin treatment (-/+TNFα pre-conditioning) they actively participate in barrier regulation throughout the time course, although the kinases and/or signaling pathways that they interact with are altered with TNFα pre-conditioning (Fig. S8, Fig. S9). Overall, the accuracy of TREKING predictions vary by specific kinase. For example, active SRC, p38 MAPK and PDPK1 were observed by western blot at most time points predicted by TREKING, but TREKING failed to make predictions on AKT1 in the presence of TNFα, perhaps due to the complexity of cell signaling through this extensively connected kinase (Fig. S5B).

Most previous and ongoing research has focused on certain stages of barrier perturbation or sampled sparsely during a time course. We therefore asked how TREKING predictions compared to the existing literature in their breadth and temporal resolution. To do this, we visualized portions of the phosphosignaling network that had been described in the literature to regulate the endothelial barrier in response to thrombin (STAR Methods, Table S4). We then performed the same visualization with kinases that had been predicted by tKiR, and finally, by TREKING. When comparing to the literature, TREKING substantially increased the number of kinases associated with thrombin-induced barrier regulation and was able to assemble most predicted kinases into a time-resolved phosphosignaling network (Fig. 7). This

highlights the power of TREKING to broadly dissect the functionally important phophosignaling, with high temporal resolution, in barrier regulation.

DISCUSSION

Kinase signaling pathways are highly implicated in endothelial barrier regulation (Komarova et al., 2017; Kuppers et al., 2014; Mehta and Malik, 2006) and consequently kinase inhibitors are being explored for treatment of vascular injury (Aman et al., 2012; Botros et al., 2020; Rizzo et al., 2015). However, a lack of resolution that describes the barrier activity of specific kinase signaling networks and their importance in barrier disruption and repair has hindered therapeutic applications. Here, we introduce TREKING, which uses kinase regression to broadly interrogate kinase signaling pathways involved in barrier regulation with temporal resolution and to study their interconnectedness in signaling networks.

In agreement with previous work (Mehta and Malik, 2006), our results using tKiR implicated multiple MAPK signaling pathways in thrombin-induced barrier changes. Because of the systematic nature of the tKiR, it was possible to assign barrier functions to specific MAPK pathways with ERK and JNK pathways involved in early barrier disruption and the p38 pathway in a mid-to-late acting barrier restoration. In each case, multiple kinases within each pathway were predicted and the barrier phenotypes followed the expected flow of phosphosignaling in the linear cascade, and kinase activation by western blots was consistent with these predictions. Beyond MAPKs, our findings highlight the complexity of endothelial barrier regulation with over 100 kinases were predicted to regulate thrombin-induced change of barrier integrity. With tKiR, “druggable windows” of the key kinase regulators mediating barrier permeability can be identified, which provides valuable insight into designing therapeutic interventions to block barrier leakage and restore barrier functionality, or in some circumstances, to temporarily disrupt the barrier for controlled drug delivery into the brain (Hashimoto et al., 2020; Luo and Shusta, 2020; Yanagida et al., 2017).

Kinase activity is frequently inferred by assessing phosphorylation via western blot or mass spectrometry. However, kinase activity is distinct from function and many kinases play multiple distinct biological roles by targeting different sets of substrates with different kinetics. While this behavior was coined “moonlighting”, suggesting there was one “main” kinase function with other ancillary activities, our data suggests that instead kinases can have multiple, equally important, and sometimes opposing functions in regulating the barrier. Since TREKING predicts functionality, rather than enzymatic activity, our work highlights these higher-order, complex activities of kinases. By reconstructing networks with temporal resolution, TREKING enables us to systematically dissect the “functional windows” of the kinases associated with barrier regulation.

We termed a subset of kinases “switch kinases”, as TREKING predicted their functionality to be barrier-weakening and barrier-strengthening during different kinetic windows. As one example of a switch kinase, MAPKAPK2/MK2 was predicted to be barrier-weakening during barrier disruption and then to switch to barrier-strengthening during late barrier recovery. MAPKAPK2/MK2 is phosphorylated and activated by MAPK14/p38α upon activation of the p38 pathway. Activation of MAPKAPK2/MK2 leads to phosphorylation of LIMK1 and heat shock protein beta-1 (HSPB1), both of which regulate actin filament dynamics in endothelial cells (Gorovoy et al., 2005; Rada et al., 2021). Together, this suggests that the p38 pathway may regulate cytoskeleton remodeling during both barrier disruption and repair through different signaling pathways. The temporal functionality of kinases in the MAP3K20/ZAK-MAPK14/p38α-MAPKAPK2/MK2 axis of the p38 pathway is coherent in response to thrombin alone, as highlighted by our SOM analysis, where all three kinases were predicted to be barrier-strengthening during mid-to-late barrier recovery. In contrast, with TNFα pre-conditioning, MAPKAPK2/MK2 no longer promotes barrier strengthening but retains its early barrier-weakening function. In parallel, we no longer observe MAPKAPK2/MK2 signaling through p38

pathway in this setting. Interestingly, our identifying of switch kinases could explain reports of kinases having contradictory activities. For instance, Src has been described to have both barrier-weakening and barrier-strengthening properties (Birukova et al., 2013; Garcia et al., 2001; Han et al., 2013; Klomp et al., 2019; Knezevic et al., 2009; McVerry and Garcia, 2004; Vouret-Craviari et al., 2002). Our model suggests that these disparate reports might simply be describing different barrier signaling activities that are kinetically resolved.

Several examples illustrate additional molecular and kinetic details that can be obtained from TREKING in contrast to traditional, less systematic approaches, including shifts in the timing of core MAPK signaling pathways (ERK/JNK pathways), condition-specific phosphosignaling networks (e.g., MAPKAPK2/MK2 switch kinase), and a skewing of barrier signaling activities at the major signaling hubs (e.g., AKT1) that alters the biological function of a key regulatory kinase. TREKING also highlights functional kinetics of cascades that are altered in TNFα pre-conditioned cells, suggesting how long-term inflammatory signals may alter the phosphosignaling network topology towards different barrier tolerances. These differences are often buried by conventional investigations that use tools such as genetic knockdown or knockout, which respond on the time scale of days rather than minutes. This highlights the importance of developing tools to systematically study the molecular details of kinase-driven signaling and to capture the differences in cell signaling between conditions.

The global, time-resolved and mechanistic details revealed by TREKING has ramifications beyond our fundamental understanding of phosphosignaling during inflammation. Beyond controlling the vasculature, TREKING is broadly generalizable to other cellular systems, and could be applied towards developing a molecular, kinetically resolved picture of any cellular phenotype.

Limitations of the study

Despite its power to elucidate kinase signaling with temporal resolution, TREKING is not without limitations. Firstly, the kinase-compound biochemical data used for KiR contains information only on a subset of the human kinome (300 of 518 kinases) (Anastassiadis et al., 2011). To partially overcome this limitation, TREKING reconstructs phosphosignaling networks and reveals functional kinases not predicted by tKiR and therefore can fill in missing gaps by leveraging kinase proteomic datasets. As additional biochemical data is available, these models can be refined. Secondly, PhosphoSitePlus®, the knowledgebase used for building the phosphosignaling networks, despite being the most comprehensive catalog available to us, does not cover the complete kinase-substrate phosphorylation interactions in human cells, nor is it specific to endothelial cells.

ACKNOWLEDGEMENTS

We would like to thank Mary-Margaret Dols for experimental guidance. This work was funded by National Institutes of Health (NIH) grants R01 AI148802 and R61 HL154250 (to J.D.S. and A.K.).

AUTHOR CONTRIBUTIONS

Conceptualization, L.W., S.D., J.D.S., and A.K.; Funding acquisition, J.D.S. and A.K.; Investigation, L.W. and S.D.; Methodology, L.W., S.D., and K.V.; Supervision, J.D.S. and A.K.; Writing – Original Draft, L.W. with help from S.D., J.D.S. and A.K.; Writing – Review & Editing, L.W., S.D., J.D.S., and A.K.

DECLARATION OF INTERESTS

The authors declare no competing interests.

Figure 1. Pre-conditioning with TNFα exacerbated thrombin-induced barrier disruption. (A) Left: representative xCELLigence data showing barrier response to thrombin with or without TNFα pre-conditioning. Right: Quantification of the maximum change and time to 50% recovery for data on left. P-values from student's t-test are shown. (B) Graphic of KiR screen conducted with 28 kinase inhibitors for their impact on barrier permeability in thrombin treated HBMECs (-/+TNFα pre-conditioning). Monolayers of HBMECs were treated with thrombin followed at 6 minutes by kinase inhibitor treatment and barrier permeability was measured in real time using xCELLigence system. (C) Correlations of the 28 kinase inhibitors between +thrombin and TNFα pre-conditioning +thrombin conditions at different stages of barrier perturbation. Kinase inhibitors had similar but distinct impact on barrier permeability in response to thrombin with or without TNFα pre-conditioning. Area under the corresponding permeability curve (AUC) within representative time windows (10-minute) is displayed as scatter plots (blue circle: DMSO-treated; black circles: kinase inhibitor-treated; black solid line: linear fitting line excluding DMSO control; black dashed line: identity line). The time windows corresponding to the scatter plots are indicated in (A) with lavender shading. (D) Pearson correlation coefficients between AUC in +thrombin and TNFα pre-conditioning +thrombin conditions. See also Figure S1.

Figure 2. Using kinase regression to inform kinases important for barrier regulation with temporal resolution. (A) Left: schematic describing analysis of using temporal KiR (tKiR) to predict kinases important for barrier regulation. A 5-minute sliding time window was applied to the normalized cell index data from the xCELLigence assay conducted with the 28 kinase inhibitors. The elastic net regularization algorithm predicted barrier "active" kinases within the corresponding time window, based on area under the curve (AUC). Right: Venn diagram showing the total number of kinases predicted in each condition across all time windows. (B)-(C) Left: time-resolved barrier activity profiles of predicted kinases in (B) +thrombin and (C) TNFα pre-conditioning +thrombin conditions. Blue and red colors represent barrier-weakening and

barrier-strengthening functionality, respectively. Predicted kinases are hierarchically clustered using Euclidean distance metric. Right: number of kinases predicted to be barrier-weakening, barrier-strengthening, or of dual functionality across the time course ("switch kinases"). (D) Venn diagrams showing the number of kinases predicted to be barrier-weakening or barrier-strengthening at different stages of barrier perturbation. See also Table S1.

Figure 3. Temporal KiR recapitulates the phosphosignaling events in canonical MAPK pathways. Members of three canonical MAPK pathways (ERK, JNK, and p38) were predicted to regulate barrier function in thrombin treated HBMECs with or without TNFα pre-conditioning. Kinases were mapped onto the corresponding signaling cascades along with their temporal functionality profiles, where blue and red shadings represent barrier-weakening and barrier-strengthening activity, respectively. Solid arrows represent direct phosphorylation interactions reported previously and dashed arrows represent indirect or inferred interactions. See also Table S1.

Figure 4. MAPK pathways are activated in response to thrombin treatment. (A) HBMECs were stimulated with TNFα (10 ng/ml) for 21 hours. A separate set of cells was left unstimulated. Cells were then treated with thrombin (5 nM) for the indicated times. Phosphorylation of members in three canonical MAPK pathways (ERK, JNK, and p38) was probed by western blot. Cells pre-conditioned with TNFα but not treated with thrombin are labeled "0-T". Data was normalized to non-treated, media only condition ("0-M"). GAPDH was used as loading control. Arrows in ERK pathway indicate the maximum phosphorylation level among all the time points investigated in this study. (B) Comparison of western blot measurements and tKiR predictions. For each kinase, the top row is the mean fold change of its phosphorylation with respect to basal level ("0-M"), where the arrows represent the direction (↑: increase; ↓: decrease) and magnitude of the rate of fold change from the previous time point (fold change/minute) in log scale (the fold change is set to 1 if it is not considered different from the basal level); the bottom

row is the tKiR predictions on the temporal barrier activity of kinases, with blue and red representing barrier-weakening and barrier-strengthening functionality, respectively. White indicates the kinase was not predicted by tKiR. “NE” stands for “not evaluated” by tKiR, since kinase inhibitors were added six minutes after thrombin treatment and no model predictions were done within that time window. Purple represents instances where different p38 kinases with barrier-weakening or barrier-strengthening functionality were predicted at that time point. See also Figure S4 and Table S3.

Figure 5. Building local phosphosignaling networks that describe thrombin-mediated barrier regulation. (A) Self-organizing map (SOM) of kinases predicted in response to thrombin without TNFα pre-conditioning (30 neurons). In each neuron, the black line is the mean functionality of all the kinases within that neuron, with “+1” indicating all kinases are barrier-strengthening and “-1” indicating all kinases are barrier-weakening. Blue and red shadings represent barrier-weakening and barrier-strengthening functionality, respectively. (B) A representative barrier-weakening neuron containing barrier-weakening kinases of similar temporal barrier kinetics. (C) A representative barrier-strengthening-dominant neuron containing barrier-strengthening kinases of similar temporal barrier kinetics, as well as a switch kinase (MAPKAPK2/MK2). (D) The local phosphosignaling network reconstructed from neuron (5,5). Kinases predicted by tKiR are labeled in orange. Kinases and connections associated with MAPK signaling, Src-family signaling and NF-κB signaling are highlighted in pink, yellow and cyan, respectively. See also Figure S2 and Table S2.

Figure 6. TREKING predicts kinase regulators and kinase-mediated signaling pathways functionally important for barrier regulation. (A) Left: comparison of western blot measurements, tKiR predictions and TREKING predictions on a subset of kinases involved in thrombin-induced barrier regulation. For each kinase, the top row is the mean fold change of its phosphorylation with respect to basal level (non-treated, media only), where the arrows

represent the direction (↑: increase; ↓: decrease) and magnitude of the rate of fold change from the previous time point (fold change/minute) in log scale (the fold change is set to 1 if it is not considered different from the basal level); the middle and bottom rows are the tKiR and TREKING predictions on the temporal barrier activity of kinases, with black representing being predicted by the models to be functional (barrier-weakening, barrier-strengthening, or dual functionality) and white representing not being predicted by the models. “NE” stands for “not evaluated”. Right: connectivity (in/out-degrees of freedom) of kinases in the composite TREKING network. Light orange and orange represent in- and out-degrees of freedom in +thrombin condition, respectively; light red and red represent in- and out-degrees of freedom in TNFα pre-conditioning +thrombin condition, respectively. (B) Overall prediction accuracy of TREKING compared to random models. Pink: correct predictions; gray: incorrect predictions. See also Figures S4 and S5, Tables S1, S2 and S3.

Figure 7. tKiR and TREKING expand the current understanding of kinases and associated phosphosignaling in barrier regulation. The reported time points in the literature were expanded to 6-minute time windows (3 minutes before/after the reported time points) to account for any experimental variations. The background network in gray includes all kinase-kinase phosphorylation interactions from the kinase-substrate phosphorylation database PhosphoSitePlus®. Blue and red nodes are the kinases reported by literature or predicted by tKiR to have barrier-weakening and barrier-strengthening functionality, respectively; purple nodes are the kinases having conflicting literature reports. Blue and red edges are the interactions predicted by TREKING that are associated with only barrier-weakening and barrier-strengthening activity, respectively; purple edges are the interactions associated with both barrier-weakening and barrier-strengthening activities. The “combined” panel in the bottom is the composite literature reports or model predictions across all time points. See also Table S4 and Supplemental file 1.

STAR★METHODS

RESOURCE AVAILABILITY

Lead contact

Further information and requests for resources and reagents should be directed to and will be fulfilled by the lead contact, Alexis Kaushansky (alexis.kaushansky@seattlechildrens.org).

Materials available

This study did not generate new unique reagents.

Data and code availability

Codes and data generated in this study are included in supplemental information.

EXPERIMENTAL MODEL AND SUBJECT DETAILS

Cell lines

Primary human brain microvascular endothelial cells (HBMECs; Cell Systems Cat# ACBRI 376) were cultured on collagen (5 µg/cm^2; Corning Cat# 354236) in HBMEC culture media (Lonza Cat# CC-3202) at 37°C and 5% CO_2. HBMECs were used until passage 9.

METHOD DETAILS

xCELLigence data acquisition

The kinetic data in this study are published and were acquired from xCELLigence assays (Dankwa et al. 2021), which are described here in brief. HBMECs were grown to confluency in xCELLigence e-plates. On the day of the assay, HBMECs were equilibrated in serum-free culture media for 1-2 hours, and thrombin was added at 5 nM. To capture thrombin-induced barrier disruption, the cell index was measured every minute for 6 minutes, after which kinase inhibitors were added in triplicate at 0.5 µM. The cell index was then measured every minute for

2 hours and thereafter, every 5 minutes for 4 hours. The assays with TNFα pre-conditioning were performed identically except that HBMECs were activated with 10 ng/ml TNFα for ~22 hours before media equilibration. Data analysis was performed as described previously (Dankwa et al. 2021) with some modifications. The cell index was normalized to baseline (0) at the time point prior to addition of thrombin and area under the curve (AUC) was determined for each kinase inhibitor treatment. For this study, the AUC was determined within 5-minute sliding windows over the 6-hour time course. AUC values were normalized by subtracting the AUC of cells treated with thrombin+DMSO or TNFα pre-conditioning +thrombin+DMSO. These values were then linearly transformed, with the most negative normalized AUC value within a 5-minute window being set to 0 and the normalized value for the control sample being set to 100.

Lysate preparation

HBMECs were seeded in 6-well plates at 55,000 cells/well and grown for 3 days. Cells were then activated with 10 ng/ml TNFα for 21 hours or kept in fresh media for the same period. On the day of lysate preparation, cells were equilibrated in serum-free culture media for 1 hour and then treated with thrombin at a final concentration of 5 nM for 5, 15, 30, 60, 120, 180, 240, 360 minutes. After the indicated incubation periods, cells were washed twice with ice-cold phosphate buffered saline (PBS) and lysed in sodium dodecyl sulfate (SDS) lysis buffer (50 mM Tris-HCl, 2% SDS, 5% glycerol, 5 mM ethylenediaminetetraacetic acid, 1 mM sodium fluoride, 10 mM β-glycerophosphate, 1 mM phenylmethylsulfonyl fluoride, 1 mM sodium orthovanadate, 1 mM dithiothreitol, supplemented with a cocktail of protease inhibitors (Roche Cat# 4693159001) and phosphatase inhibitors (Sigma-Aldrich Cat# P5726)). Cell lysates were clarified in filter plates at 3500 rpm for 30 minutes, after which they were stored at -80°C until use.

Western blot

All the gel electrophoresis was performed using Bolt™ 4-12% Bis-Tris mini protein gels. Proteins were transferred to PVDF membranes using iBlot 2 dry blotting system (Thermo Fisher

Scientific Cat# IB21001). Primary antibodies were used at concentrations recommended by the vendor (see Table S3 for antibody dilutions). Antibody to GAPDH (Cell Signaling Technology Cat# 97166) was used as loading control at 1:2000 dilution. Blots were imaged using Bio-Rad ChemiDoc imaging system and signals were quantified using ImageJ2 (version 2.3.0). Background correction was done for each band by subtracting background signals nearby the band. The signals from proteins of interest were first normalized to the signals from GAPDH, and then the signals at each time point were normalized to the signals at time zero for the fold change of phosphorylation from basal level.

Elastic net regularization

The elastic net regularization algorithm used for this study was published previously (Dankwa et al. 2021). For each time window, the algorithm was applied on the normalized AUC values and kinases with non-zero coefficients were predicted to be informative for barrier permeability. The sign of the coefficients indicates the functionality of the kinases in regulating barrier integrity, with kinases having positive and negative coefficients being informed to have barrier-strengthening and barrier-weakening function, respectively.

Self-organizing map

The NumPy-based SOM implementation MiniSom (https://github.com/JustGlowing/minisom) was used to cluster the tKiR predicted kinases by their temporal characteristics. Grid size of 6×6 was used to generate SOMs.

Path search

Search for the shortest paths between kinases was done using NetworkX (https://github.com/networkx/networkx), a Python package for analyzing complex network structures.

Generation of random models

The random models were generated following the TREKING pipeline. During each iteration, a random background phosphosignaling network was generated using the configuration model function in NetworkX package, which creates random directed graphs with given degree sequences. The random network contains 518 nodes, corresponding to the total number of human protein kinases, and the in- and out-degree sequences followed the same distribution as the background phosphosignaling network used in TREKING. All the kinases were shuffled and randomly assigned to each of the nodes in the random network. At each time point, kinases of barrier-weakening or barrier-strengthening functionality were randomly selected from the 300 kinases used for KiR, with probabilities the same as in the TREKING model at the corresponding time point. The random sampling of kinases was performed at all time points corresponding to the TREKING model. Each of the kinases selected at any time point during the time course was randomly assigned to one of the 36 clusters, corresponding to the total number of neurons generated by SOMs. For each cluster the phosphosignaling network was reconstructed by searching for the shortest paths between any pair of kinases within the cluster, using the random phosphosignaling network generated during the iteration as the background network. In total, 100 random models were generated and used to compare with TREKING predictions.

Literature search

To compare the scope of previous research with the current study, a comprehensive literature search on protein kinases reported to regulate barrier function was done using the free search engine PubMed (https://pubmed.ncbi.nlm.nih.gov). The search terms were “endothelial barrier thrombin” plus kinase gene names, and the search results were filtered so that only articles published on or after year 2000 were shown. The search was done on each of the 518 human protein kinases. The search was not restricted to studies on HBMECs; instead, studies on thrombin-induced barrier disruption using endothelial cell lines, primary endothelial cells isolated

from different organs, or *in vivo* studies using mice or rats, were all included. To compare with our work, studies or data beyond a 6-hour time window (after thrombin treatment) were excluded.

Visualization

Schematics were created with BioRender.com. Phosphosignaling networks were visualized using Cytoscape (https://cytoscape.org), with the hierarchic layout from yFiles layout algorithms (https://www.yworks.com/products/yfiles-layout-algorithms-for-cytoscape).

QUANTIFICATION AND STATISTICAL ANALYSIS

Statistical analysis

Student's t-test was used to evaluate the difference of kinase activity between non-treated and thrombin-treated conditions. SciPy statistical package was used to perform the t-tests. At each time point, both p-value and fold change of phosphorylation with respect to non-treated cells were reported to determine if the two sets of data are different from each other. A p-value below 0.05 or all biological replicates reporting a fold change increasing/decreasing by at least 20% compared to non-treated cells indicates that the kinase activity is different between non-treated and thrombin-treated conditions.

SUPPLEMENTAL INFORMATION

Figure S1. Workflow for building TREKING models from tKiR predictions, related to STAR Methods. Top: temporal kinase functionality was predicted using the elastic net regularization algorithm. Kinase inhibitor screen data (Dankwa et al., 2021) and kinase-compound biochemical data (Anastassiadis et al., 2011) were used for tKiR. Temporal AUC was calculated within a 5-minute sliding time window that slides at 1-minute steps for the first 2 hours of kinase inhibitor treatment and at 5-minute steps afterwards. The direction of barrier activity of kinases (barrier-weakening or barrier-strengthening functionality) was predicted at each time window indicated above based on the slope of the 28 kinase inhibitors AUC values versus the residual kinase activity from the Anastassiadis et al dataset. Middle: workflow for building TREKING networks to describe kinase phosphosignaling in thrombin-activated barriers. Self-organizing maps (SOMs) were used to identify kinases with similar time-resolved barrier activity across the 6-hour timeframe following thrombin treatment. Local phosphosignaling networks for each neuron were built by searching for the shortest paths between any pair of kinases within that neuron using the kinase-kinase phosphorylation database on PhosphoSitePlus® as the background network. Bottom: for a subset of kinases in the tKiR and TREKING models, their phosphorylation levels were measured by western blot at multiple time points in the barrier disruption and barrier recovery phases. Western blot measurements were used to evaluate if tKiR and TREKING correctly predicted the functional associations of these kinases in thrombin-induced barrier perturbation.

Figure S2. Build local phosphosignaling networks based on kinase functional kinetics, related to Figure 5. (A) Self-organizing map (SOM) of kinases predicted in TNFα pre-conditioning +thrombin condition (35 neurons). In each neuron, the black line is the mean functionality of all the kinases within that neuron, with “+1” indicating all kinases are barrier-strengthening and “-1” indicating all kinases are barrier-weakening. Blue and red shadings

represent barrier-weakening and barrier-strengthening functionality, respectively. (B)-(C) Distance maps of SOM clustering in (B) +thrombin and (C) TNFα pre-conditioning +thrombin conditions. Each cell is the normalized sum of the Euclidean distances between a neuron and its neighboring neurons. (D) Distribution of the number of kinases assigned to the SOM neurons. (E) Left: example of how a local phosphosignaling network was built for each neuron by searching for the shortest paths between any pair of kinases within that cluster using the kinase-kinase phosphorylation database on PhosphoSitePlus® as the background network. Right: the maximum path length in the local phosphosignaling networks.

Figure S3. TNFα pre-conditioning altered the key kinase regulators and skewed the signaling networks towards barrier-weakening activities in the barrier disruption phase. (A) Venn diagram showing the tKiR predicted barrier-weakening kinases during the barrier disruption phase (6-30 minutes after thrombin treatment). (B) Connectivity (in/out-degrees of freedom) of kinases functional in the barrier disruption phase in +thrombin (top) and TNFα pre-conditioning +thrombin (bottom) conditions. Blue and red represent connections associated with only barrier-weakening and barrier-strengthening activities, respectively; gray represents connections associated with both barrier-weakening and barrier-strengthening activities. (C) Left: network connections to and from AKT1 in the barrier disruption phase in +thrombin (top) and TNFα pre-conditioning +thrombin (bottom) conditions. Blue and red represent connections associated with only barrier-weakening and barrier-strengthening activities, respectively; gray represents connections associated with both barrier-weakening and barrier-strengthening activities. Right: connectivity of AKT1 in the TREKING network reconstructed in the barrier disruption phase.

Figure S4. Summary of western blot measurements performed in this study, related to Figures 4 and 6. The kinases are ordered according to their network connectivity (low to high). Left: functionality profiles predicted by TREKING. For each kinase of interest, the mean

functionality profiles of all the associated neurons in the composite TREKING network were pooled and displayed on the same graph (orange: +thrombin condition; red: TNFα pre-conditioning +thrombin condition). Middle: fold change of phosphorylation in +thrombin condition; right: fold change of phosphorylation in TNFα pre-conditioning +thrombin condition. GAPDH was used as loading control.

Figure S5. Evaluate the accuracy of TREKING predictions using western blot, related to Figure 6. (A) For each kinase, the mean functionality profiles of all the associated neurons in the composite TREKING network were pooled. Within a 10-minute time window centered at the designated time point, the kinase is functionally active if TREKING predicts its activity in any of the neurons or associated networks within the time window. In each experimental condition, the kinase phosphorylation after thrombin treatment was compared to its phosphorylation at basal level (media only) to determine if the kinase is activated in response to thrombin. If TREKING predicted the kinase to be functional at a given time, and the kinase activity as measured by western blot is different from cells not treated with thrombin (i.e., higher or lower than basal level), the model made correct predictions on its functionality in barrier regulation; otherwise, the model failed to make predictions on its functionality at the corresponding time point. (B) Summary of model validations in +thrombin (left) and TNFα pre-conditioning +thrombin (right) conditions. Pink indicates that TREKING correctly predicted the kinase functionality in barrier regulation and grey indicates incorrect predictions. Kinase connectivity (in/out-degrees of freedom) in the composite TREKING network is shown to the right of the panel. Light orange and orange represent in- and out-degrees of freedom in +thrombin condition, respectively; light red and red represent in- and out-degrees of freedom in TNFα pre-conditioning +thrombin condition, respectively. (C)-(D) Comparison of TREKING and random models in (C) +thrombin and (D) TNFα pre-conditioning +thrombin conditions. Top: accuracy of model predictions for

each kinase across the time course; bottom: accuracy of model predictions at each time window for kinases evaluated in this study.

Figure S6. Composite TREKING network for the barrier disruption phase in +thrombin condition. Kinases predicted by tKiR are labeled in blue (barrier-weakening) and red (barrier-strengthening). Blue and red lines represent connections associated with only barrier-weakening and barrier-strengthening activities, respectively; gray lines represent connections associated with both barrier-weakening and barrier-strengthening activities.

Figure S7. Composite TREKING network for the barrier disruption phase in TNFα pre-conditioning +thrombin condition. Kinases predicted by tKiR are labeled in blue (barrier-weakening) and red (barrier-strengthening). Blue and red lines represent connections associated with only barrier-weakening and barrier-strengthening activities, respectively; gray lines represent connections associated with both barrier-weakening and barrier-strengthening activities.

Figure S8. Composite TREKING network for the entire 6-hour time course in +thrombin condition. Kinases predicted by tKiR in the barrier disruption phase are labeled in blue (barrier-weakening) and red (barrier-strengthening); kinases predicted by tKiR in the barrier recovery and plateau phases are labeled in light blue (barrier-weakening) and light red (barrier-strengthening); switch kinases are labeled in gray. Blue and red lines represent connections associated with only barrier-weakening and barrier-strengthening activities, respectively; gray lines represent connections associated with both barrier-weakening and barrier-strengthening activities.

Figure S9. Composite TREKING network for the 6-hour time course in response to TNFα pre-conditioning +thrombin. Kinases predicted by tKiR in the barrier disruption phase are labeled in blue (barrier-weakening) and red (barrier-strengthening); kinases predicted by tKiR in the barrier recovery and plateau phases are labeled in light blue (barrier-weakening) and light

red (barrier-strengthening); switch kinases are labeled in gray. Blue and red lines represent connections associated with only barrier-weakening and barrier-strengthening activities, respectively; gray lines represent connections associated with both barrier-weakening and barrier-strengthening activities.

Table S1. Predicted temporal kinase functionality in +thrombin and TNFα pre-conditioning +thrombin conditions, related to Figure 2. This is a Microsoft Excel workbook containing two spreadsheets.

Table S2. SOM assignment of tKiR predicted kinases and edges of phosphosignaling networks built in +thrombin and TNFα pre-conditioning +thrombin conditions, related to Figure 5. This is a Microsoft Excel workbook containing four spreadsheets.

Table S3. Antibody information and western blot results on the kinases validated in this study, related to Figures 4 and 6. This is a Microsoft Excel workbook containing 14 spreadsheets.

Table S4. Literature search on protein kinases reported to regulate endothelial barrier integrity in response to thrombin, related to Figure 7. PubMed ID of the article is followed by the barrier functionality reported in the corresponding article ("-1": barrier-weakening; "1": barrier-strengthening). This is a Microsoft Excel workbook containing one spreadsheet.

Supplemental file 1. Movie comparing literature reported with tKiR and TREKING predicted kinases and signaling pathways important for barrier regulation. This is an MPEG-4 movie file.

Supplemental file 2. Jupyter notebook containing the scripts for tKiR, SOM generation and network construction. Also including the scripts for making frames for the supplemental movie (Supplemental file 1) and random model generation.

REFERENCES

Aman, J., van Bezu, J., Damanafshan, A., Huveneers, S., Eringa, E.C., Vogel, S.M., Groeneveld, A.B., Vonk Noordegraaf, A., van Hinsbergh, V.W., and van Nieuw Amerongen, G.P. (2012). Effective treatment of edema and endothelial barrier dysfunction with imatinib. Circulation *126*, 2728-2738.

Anastassiadis, T., Deacon, S.W., Devarajan, K., Ma, H., and Peterson, J.R. (2011). Comprehensive assay of kinase catalytic activity reveals features of kinase inhibitor selectivity. Nat Biotechnol *29*, 1039-1045.

Anrather, D., Millan, M.T., Palmetshofer, A., Robson, S.C., Geczy, C., Ritchie, A.J., Bach, F.H., and Ewenstein, B.M. (1997). Thrombin activates nuclear factor-kappaB and potentiates endothelial cell activation by TNF. J Immunol *159*, 5620-5628.

Arang, N., Kain, H.S., Glennon, E.K., Bello, T., Dudgeon, D.R., Walter, E.N.F., Gujral, T.S., and Kaushansky, A. (2017). Identifying host regulators and inhibitors of liver stage malaria infection using kinase activity profiles. Nat Commun *8*, 1232.

Beguin, E.P., van den Eshof, B.L., Hoogendijk, A.J., Nota, B., Mertens, K., Meijer, A.B., and van den Biggelaar, M. (2019). Integrated proteomic analysis of tumor necrosis factor alpha and interleukin 1beta-induced endothelial inflammation. J Proteomics *192*, 89-101.

Birukova, A.A., Tian, X., Tian, Y., Higginbotham, K., and Birukov, K.G. (2013). Rap-afadin axis in control of Rho signaling and endothelial barrier recovery. Mol Biol Cell *24*, 2678-2688.

Botros, L., Pronk, M.C.A., Juschten, J., Liddle, J., Morsing, S.K.H., van Buul, J.D., Bates, R.H., Tuinman, P.R., van Bezu, J.S.M., Huveneers, S.*, et al.* (2020). Bosutinib prevents vascular leakage by reducing focal adhesion turnover and reinforcing junctional integrity. J Cell Sci *133*.

Casado, P., Rodriguez-Prados, J.C., Cosulich, S.C., Guichard, S., Vanhaesebroeck, B., Joel, S., and Cutillas, P.R. (2013). Kinase-substrate enrichment analysis provides insights into the heterogeneity of signaling pathway activation in leukemia cells. Sci Signal *6*, rs6.

Daneman, R., and Prat, A. (2015). The blood-brain barrier. Cold Spring Harb Perspect Biol *7*, a020412.

Dankwa, S., Dols, M.M., Wei, L., Glennon, E.K.K., Kain, H.S., Kaushansky, A., and Smith, J.D. (2021). Exploiting polypharmacology to dissect host kinases and kinase inhibitors that modulate endothelial barrier integrity. Cell Chem Biol.

Garcia, J.G., Liu, F., Verin, A.D., Birukova, A., Dechert, M.A., Gerthoffer, W.T., Bamberg, J.R., and English, D. (2001). Sphingosine 1-phosphate promotes endothelial cell barrier integrity by Edg-dependent cytoskeletal rearrangement. J Clin Invest *108*, 689-701.

Gorovoy, M., Niu, J., Bernard, O., Profirovic, J., Minshall, R., Neamu, R., and Voyno-Yasenetskaya, T. (2005). LIM kinase 1 coordinates microtubule stability and actin polymerization in human endothelial cells. J Biol Chem *280*, 26533-26542.

Gujral, T.S., Peshkin, L., and Kirschner, M.W. (2014). Exploiting polypharmacology for drug target deconvolution. Proc Natl Acad Sci U S A *111*, 5048-5053.

Guo, H., Zhou, H., Lu, J., Qu, Y., Yu, D., and Tong, Y. (2016). Vascular endothelial growth factor: an attractive target in the treatment of hypoxic/ischemic brain injury. Neural Regen Res *11*, 174-179.

Han, J., Zhang, G., Welch, E.J., Liang, Y., Fu, J., Vogel, S.M., Lowell, C.A., Du, X., Cheresh, D.A., Malik, A.B.*, et al.* (2013). A critical role for Lyn kinase in strengthening endothelial integrity and barrier function. Blood *122*, 4140-4149.

Hashimoto, Y., Tachibana, K., and Kondoh, M. (2020). Tight junction modulators for drug delivery to the central nervous system. Drug Discov Today *25*, 1477-1486.

Hornbeck, P.V., Zhang, B., Murray, B., Kornhauser, J.M., Latham, V., and Skrzypek, E. (2015). PhosphoSitePlus, 2014: mutations, PTMs and recalibrations. Nucleic Acids Res *43*, D512-520.

Klomp, J.E., Shaaya, M., Matsche, J., Rebiai, R., Aaron, J.S., Collins, K.B., Huyot, V., Gonzalez, A.M., Muller, W.A., Chew, T.L.*, et al.* (2019). Time-Variant SRC Kinase Activation Determines Endothelial Permeability Response. Cell Chem Biol *26*, 1081-1094 e1086.

Knezevic, N., Tauseef, M., Thennes, T., and Mehta, D. (2009). The G protein betagamma subunit mediates reannealing of adherens junctions to reverse endothelial permeability increase by thrombin. J Exp Med *206*, 2761-2777.

Kohonen, T. (1982). Self-organized formation of topologically correct feature maps. Biological cybernetics *43*, 59-69.

Komarova, Y.A., Kruse, K., Mehta, D., and Malik, A.B. (2017). Protein Interactions at Endothelial Junctions and Signaling Mechanisms Regulating Endothelial Permeability. Circ Res *120*, 179-206.

Kuppers, V., Vockel, M., Nottebaum, A.F., and Vestweber, D. (2014). Phosphatases and kinases as regulators of the endothelial barrier function. Cell Tissue Res *355*, 577-586.

Liu, Y., Pelekanakis, K., and Woolkalis, M.J. (2004). Thrombin and tumor necrosis factor alpha synergistically stimulate tissue factor expression in human endothelial cells: regulation through c-Fos and c-Jun. J Biol Chem *279*, 36142-36147.

Luo, H., and Shusta, E.V. (2020). Blood-Brain Barrier Modulation to Improve Glioma Drug Delivery. Pharmaceutics *12*.

Marcos-Ramiro, B., Garcia-Weber, D., and Millan, J. (2014). TNF-induced endothelial barrier disruption: beyond actin and Rho. Thromb Haemost *112*, 1088-1102.

McVerry, B.J., and Garcia, J.G. (2004). Endothelial cell barrier regulation by sphingosine 1-phosphate. J Cell Biochem *92*, 1075-1085.

Mehta, D., and Malik, A.B. (2006). Signaling mechanisms regulating endothelial permeability. Physiol Rev *86*, 279-367.

Miller, L.H., Ackerman, H.C., Su, X.Z., and Wellems, T.E. (2013). Malaria biology and disease pathogenesis: insights for new treatments. Nat Med *19*, 156-167.

Minami, T., Sugiyama, A., Wu, S.Q., Abid, R., Kodama, T., and Aird, W.C. (2004). Thrombin and phenotypic modulation of the endothelium. Arterioscler Thromb Vasc Biol *24*, 41-53.

Morrison, D.K. (2012). MAP kinase pathways. Cold Spring Harb Perspect Biol *4*.

Oldenburg, J., and de Rooij, J. (2014). Mechanical control of the endothelial barrier. Cell Tissue Res *355*, 545-555.

Pimienta, G., and Pascual, J. (2007). Canonical and alternative MAPK signaling. Cell Cycle *6*, 2628-2632.

Rada, C.C., Mejia-Pena, H., Grimsey, N.J., Canto Cordova, I., Olson, J., Wozniak, J.M., Gonzalez, D.J., Nizet, V., and Trejo, J. (2021). Heat shock protein 27 activity is linked to endothelial barrier recovery after proinflammatory GPCR-induced disruption. Sci Signal *14*, eabc1044.

Radeva, M.Y., and Waschke, J. (2018). Mind the gap: mechanisms regulating the endothelial barrier. Acta Physiol (Oxf) *222*.

Rizzo, A.N., Aman, J., van Nieuw Amerongen, G.P., and Dudek, S.M. (2015). Targeting Abl kinases to regulate vascular leak during sepsis and acute respiratory distress syndrome. Arterioscler Thromb Vasc Biol *35*, 1071-1079.

Schafer, A., Gjerga, E., Welford, R.W., Renz, I., Lehembre, F., Groenen, P.M., Saez-Rodriguez, J., Aebersold, R., and Gstaiger, M. (2019). Elucidating essential kinases of endothelin signalling by logic modelling of phosphoproteomics data. Mol Syst Biol *15*, e8828.

Tiruppathi, C., Naqvi, T., Sandoval, R., Mehta, D., and Malik, A.B. (2001). Synergistic effects of tumor necrosis factor-alpha and thrombin in increasing endothelial permeability. Am J Physiol Lung Cell Mol Physiol *281*, L958-968.

Vaga, S., Bernardo-Faura, M., Cokelaer, T., Maiolica, A., Barnes, C.A., Gillet, L.C., Hegemann, B., van Drogen, F., Sharifian, H., Klipp, E.*, et al.* (2014). Phosphoproteomic analyses reveal

novel cross-modulation mechanisms between two signaling pathways in yeast. Mol Syst Biol *10*, 767.

van den Biggelaar, M., Hernandez-Fernaud, J.R., van den Eshof, B.L., Neilson, L.J., Meijer, A.B., Mertens, K., and Zanivan, S. (2014). Quantitative phosphoproteomics unveils temporal dynamics of thrombin signaling in human endothelial cells. Blood *123*, e22-36.

Vouret-Craviari, V., Bourcier, C., Boulter, E., and van Obberghen-Schilling, E. (2002). Distinct signals via Rho GTPases and Src drive shape changes by thrombin and sphingosine-1-phosphate in endothelial cells. J Cell Sci *115*, 2475-2484.

Yanagida, K., Liu, C.H., Faraco, G., Galvani, S., Smith, H.K., Burg, N., Anrather, J., Sanchez, T., Iadecola, C., and Hla, T. (2017). Size-selective opening of the blood-brain barrier by targeting endothelial sphingosine 1-phosphate receptor 1. Proc Natl Acad Sci U S A *114*, 4531-4536.

Zhao, Z., Nelson, A.R., Betsholtz, C., and Zlokovic, B.V. (2015). Establishment and Dysfunction of the Blood-Brain Barrier. Cell *163*, 1064-1078.

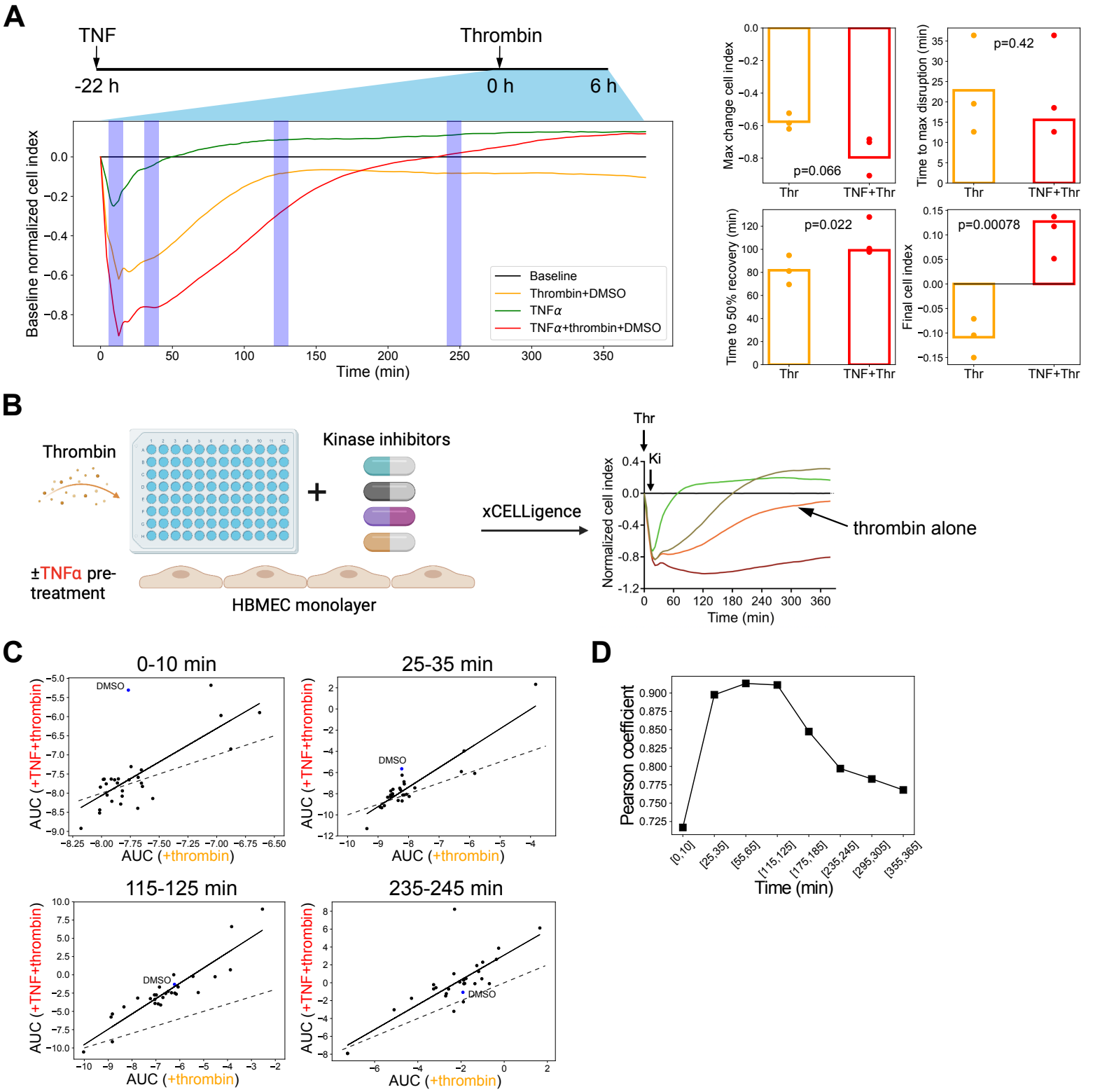
A
TNF
Thrombin
-22 h
0 h
6 h
Baseline normalized cell index
Time (min)
Baseline
Thrombin+DMSO
TNFα
TNFα+thrombin+DMSO
Max change cell index
p=0.066
Time to max disruption (min)
p=0.42
Time to 50% recovery (min)
p=0.022
Final cell index
p=0.00078
Thr
TNF+Thr
B
Thrombin
Kinase inhibitors
±TNFα pre-treatment
HBMEC monolayer
xCELLigence
Thr
Ki
Normalized cell index
thrombin alone
Time (min)
C
0-10 min
25-35 min
115-125 min
235-245 min
DMSO
AUC (+TNF+thrombin)
AUC (+thrombin)
D
Pearson coefficient
Time (min)
[0,10]
[25,35]
[55,65]
[115,125]
[175,185]
[235,245]
[295,305]
[355,365]

Figure 1

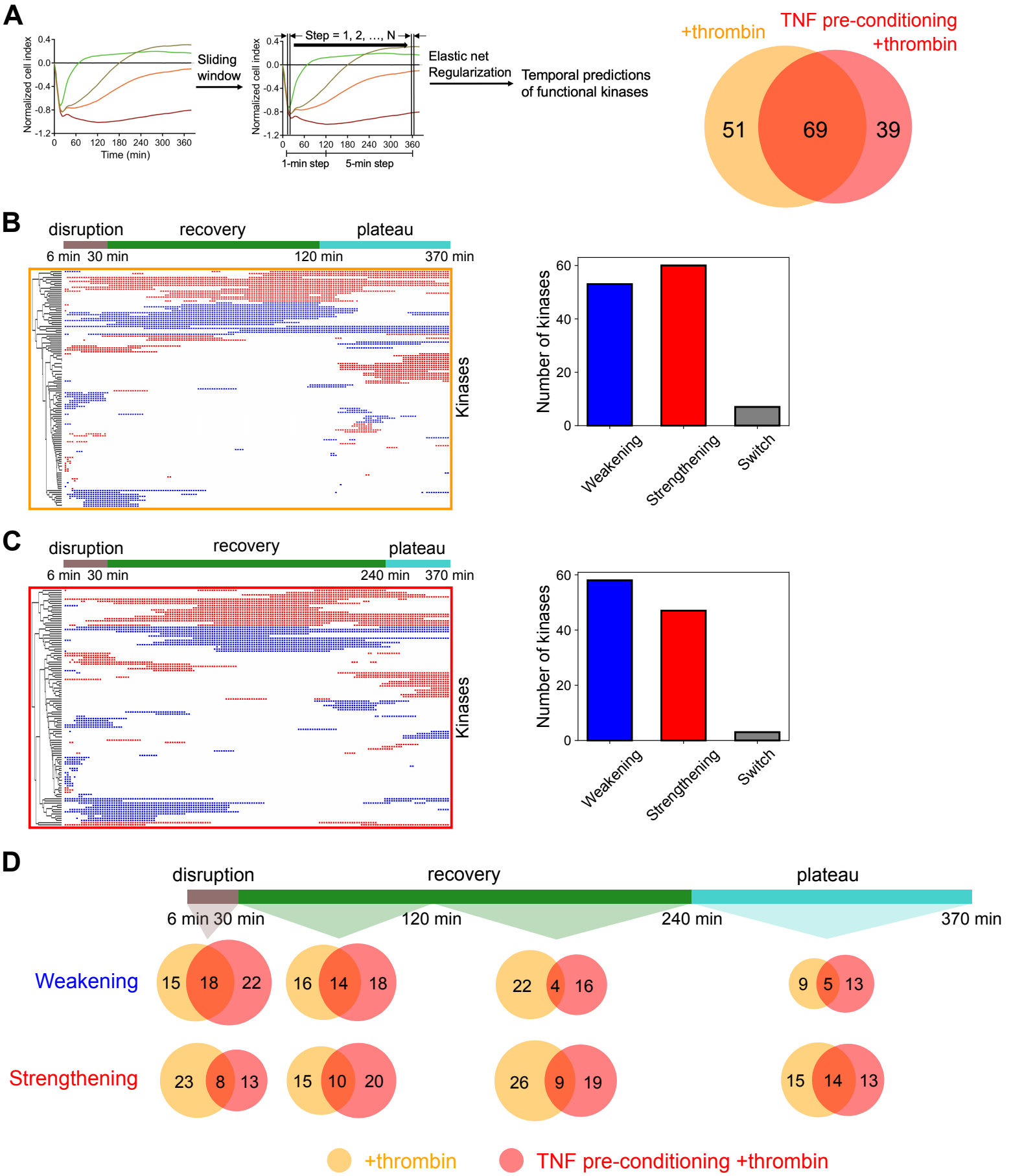
A
Normalized cell index
Time (min)
Sliding window
Step = 1, 2, …, N
1-min step
5-min step
Elastic net Regularization
Temporal predictions of functional kinases
+thrombin
TNF pre-conditioning +thrombin
51
69
39
B
disruption
recovery
plateau
6 min
30 min
120 min
370 min
Kinases
Number of kinases
Weakening
Strengthening
Switch
C
disruption
recovery
plateau
6 min
30 min
240 min
370 min
Kinases
Number of kinases
Weakening
Strengthening
Switch
D
disruption
recovery
plateau
6 min
30 min
120 min
240 min
370 min
Weakening
15 18 22
16 14 18
22 4 16
9 5 13
Strengthening
23 8 13
15 10 20
26 9 19
15 14 13
+thrombin
TNF pre-conditioning +thrombin

Figure 2

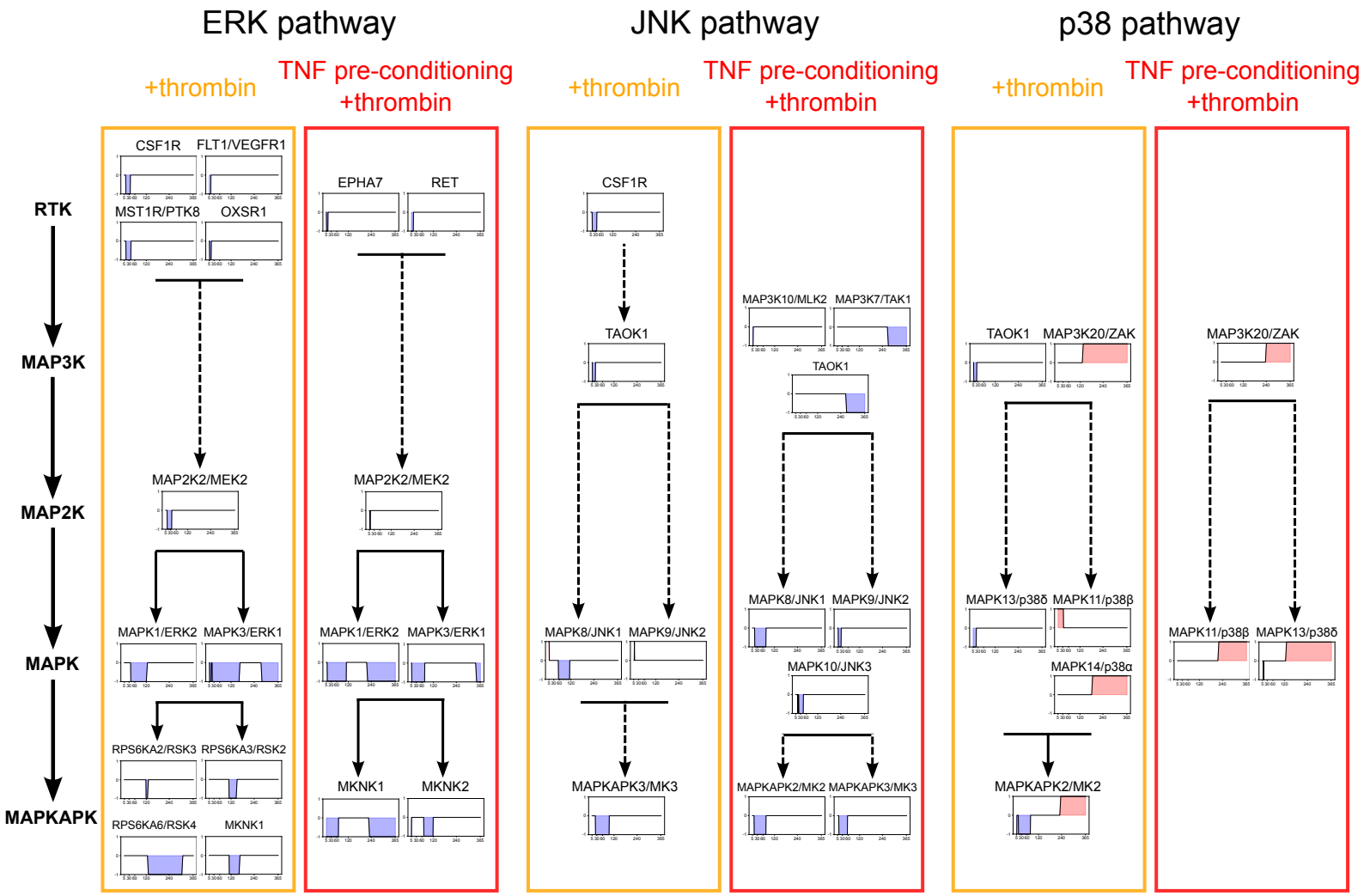
ERK pathway
JNK pathway
p38 pathway
+thrombin
TNF pre-conditioning +thrombin
+thrombin
TNF pre-conditioning +thrombin
+thrombin
TNF pre-conditioning +thrombin
RTK
MAP3K
MAP2K
MAPK
MAPKAPK
CSF1R
FLT1/VEGFR1
MST1R/PTK8
OXSR1
MAP2K2/MEK2
MAPK1/ERK2
MAPK3/ERK1
RPS6KA2/RSK3
RPS6KA3/RSK2
RPS6KA6/RSK4
MKNK1
EPHA7
RET
MAP2K2/MEK2
MAPK1/ERK2
MAPK3/ERK1
MKNK1
MKNK2
CSF1R
TAOK1
MAPK8/JNK1
MAPK9/JNK2
MAPKAPK3/MK3
MAP3K10/MLK2
MAP3K7/TAK1
TAOK1
MAPK8/JNK1
MAPK9/JNK2
MAPK10/JNK3
MAPKAPK2/MK2
MAPKAPK3/MK3
TAOK1
MAP3K20/ZAK
MAPK13/p38δ
MAPK11/p38β
MAPK14/p38α
MAPKAPK2/MK2
MAP3K20/ZAK
MAPK11/p38β
MAPK13/p38δ

Figure 3

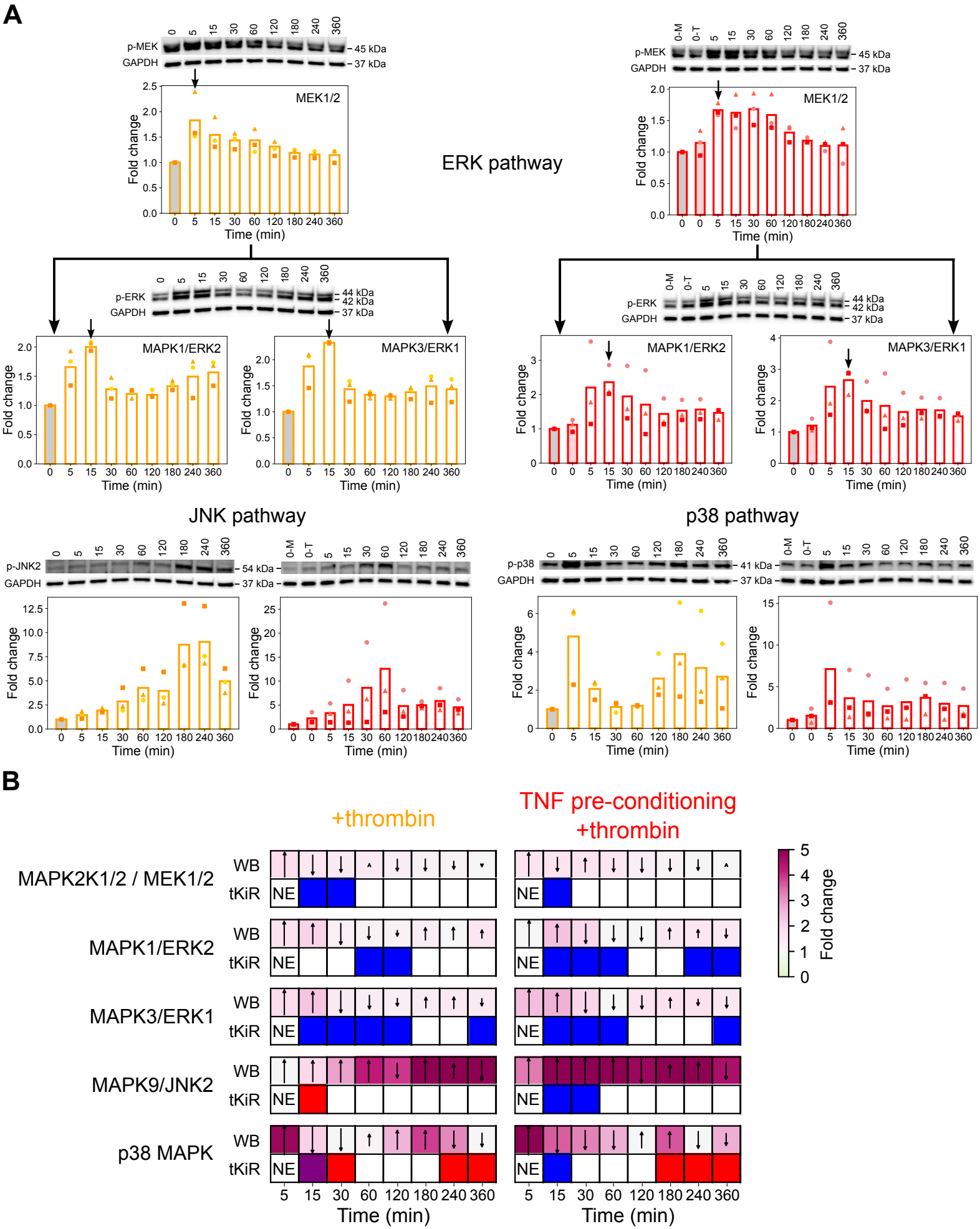
A
ERK pathway
p-MEK
GAPDH
45 kDa
37 kDa
MEK1/2
Fold change
Time (min)
p-ERK
44 kDa
42 kDa
MAPK1/ERK2
MAPK3/ERK1
JNK pathway
p38 pathway
p-JNK2
54 kDa
p-p38
41 kDa
B
+thrombin
TNF pre-conditioning
+thrombin
MAPK2K1/2 / MEK1/2
MAPK1/ERK2
MAPK3/ERK1
MAPK9/JNK2
p38 MAPK
WB
tKiR
NE
Fold change

Figure 4

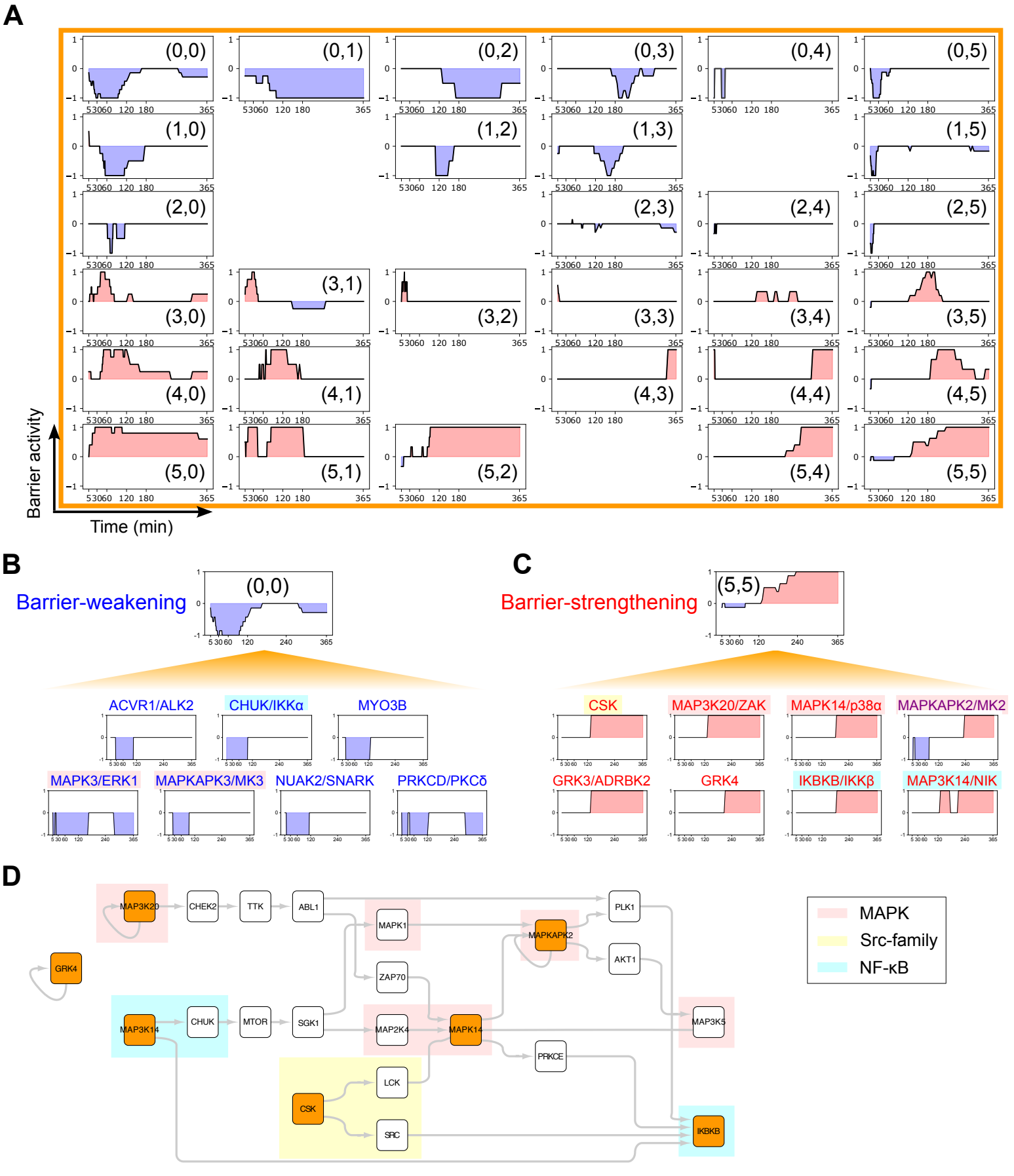
A
(0,0)
(0,1)
(0,2)
(0,3)
(0,4)
(0,5)
(1,0)
(1,2)
(1,3)
(1,5)
(2,0)
(2,3)
(2,4)
(2,5)
(3,0)
(3,1)
(3,2)
(3,3)
(3,4)
(3,5)
(4,0)
(4,1)
(4,3)
(4,4)
(4,5)
(5,0)
(5,1)
(5,2)
(5,4)
(5,5)
Barrier activity
Time (min)
B
Barrier-weakening
(0,0)
ACVR1/ALK2
CHUK/IKKα
MYO3B
MAPK3/ERK1
MAPKAPK3/MK3
NUAK2/SNARK
PRKCD/PKCδ
C
Barrier-strengthening
(5,5)
CSK
MAP3K20/ZAK
MAPK14/p38α
MAPKAPK2/MK2
GRK3/ADRBK2
GRK4
IKBKB/IKKβ
MAP3K14/NIK
D
MAP3K20
CHEK2
TTK
ABL1
MAPK1
PLK1
MAPKAPK2
AKT1
GRK4
ZAP70
MAP3K14
CHUK
MTOR
SGK1
MAP2K4
MAPK14
MAP3K5
PRKCE
LCK
CSK
SRC
IKBKB
MAPK
Src-family
NF-κB

Figure 5

A

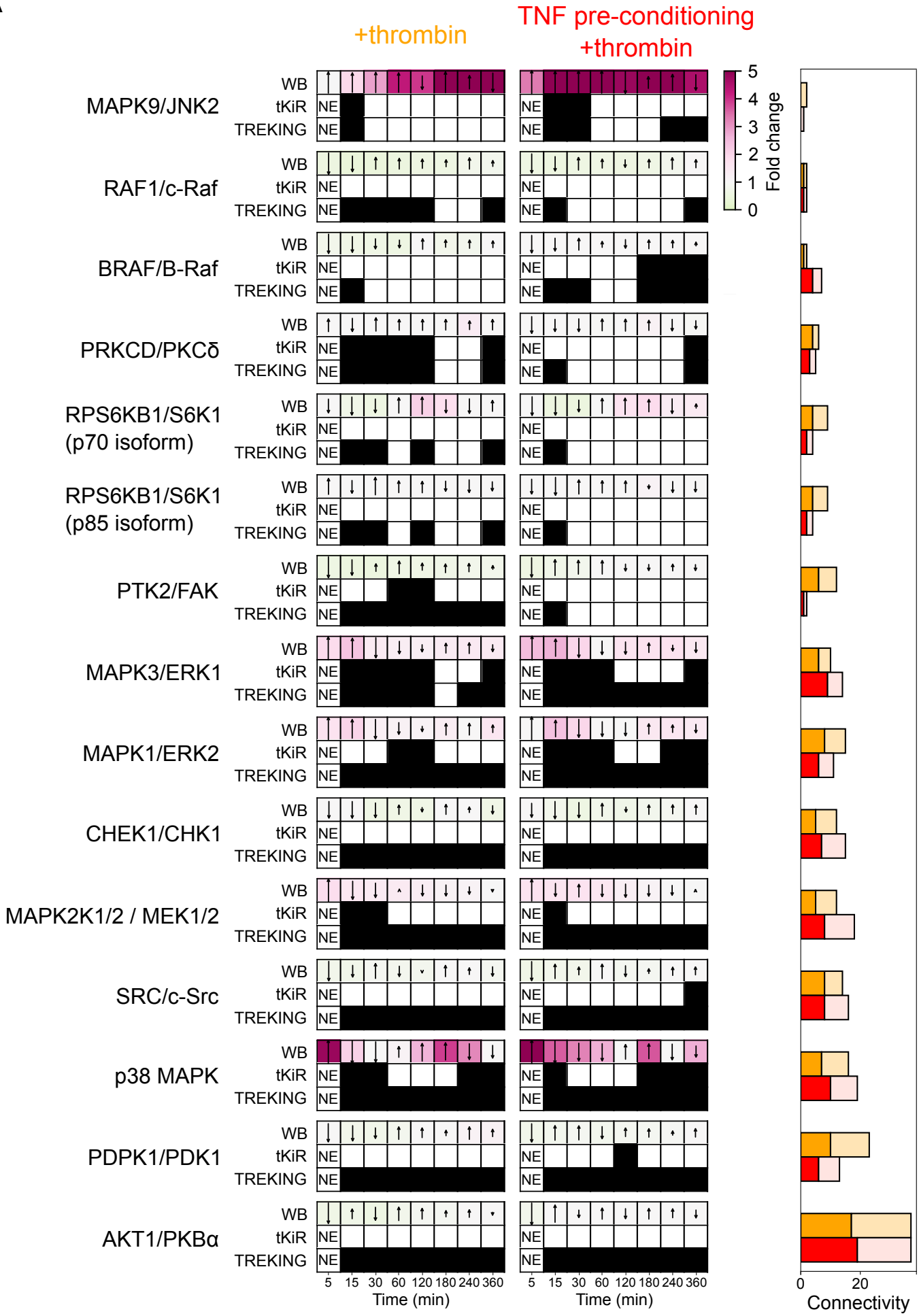
+thrombin
TNF pre-conditioning +thrombin
MAPK9/JNK2
RAF1/c-Raf
BRAF/B-Raf
PRKCD/PKCδ
RPS6KB1/S6K1 (p70 isoform)
RPS6KB1/S6K1 (p85 isoform)
PTK2/FAK
MAPK3/ERK1
MAPK1/ERK2
CHEK1/CHK1
MAPK2K1/2 / MEK1/2
SRC/c-Src
p38 MAPK
PDPK1/PDK1
AKT1/PKBα
WB
tKiR
TREKING
NE
5 15 30 60 120 180 240 360
Time (min)
Fold change
0 1 2 3 4 5
0 20
Connectivity

B

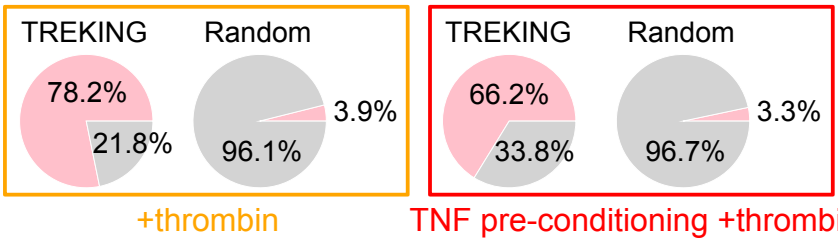
TREKING
Random
78.2%
21.8%
96.1%
3.9%
+thrombin
TREKING
Random
66.2%
33.8%
96.7%
3.3%
TNF pre-conditioning +thrombin

Figure 6

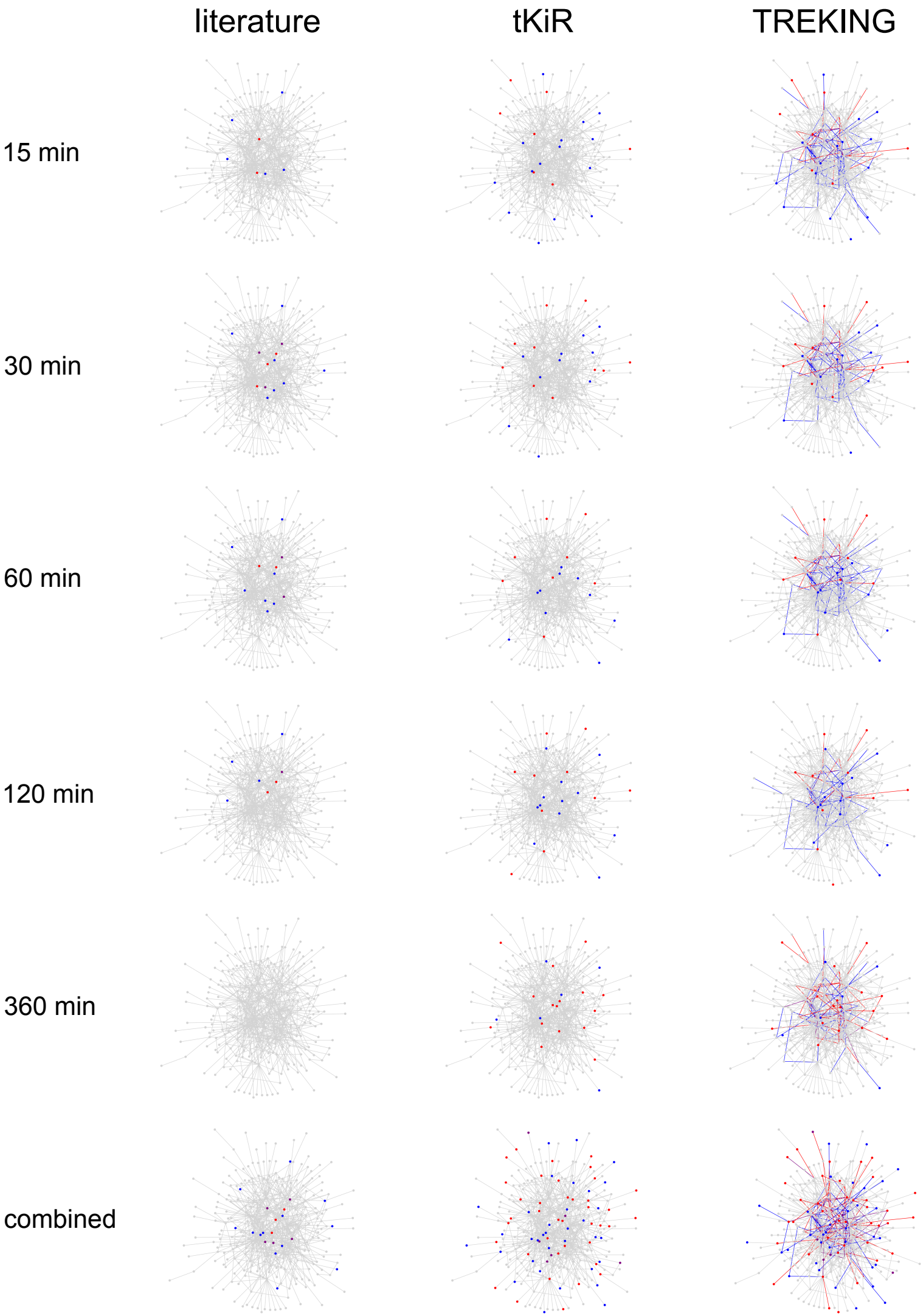
literature
tKiR
TREKING
15 min
30 min
60 min
120 min
360 min
combined

Figure 7

KiR models of temporal kinase functionality and barrier phenotypes

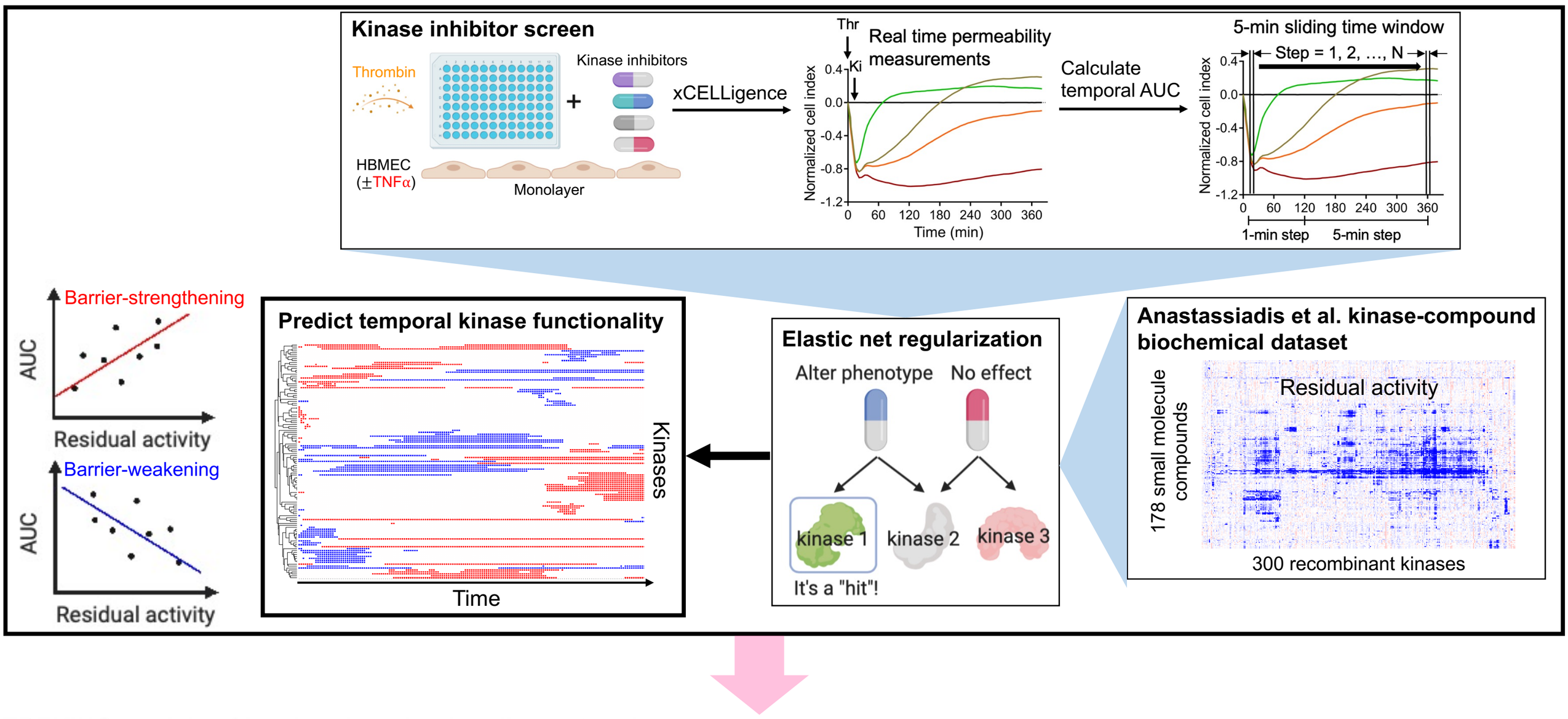

TREKING models of barrier phosphosignaling networks

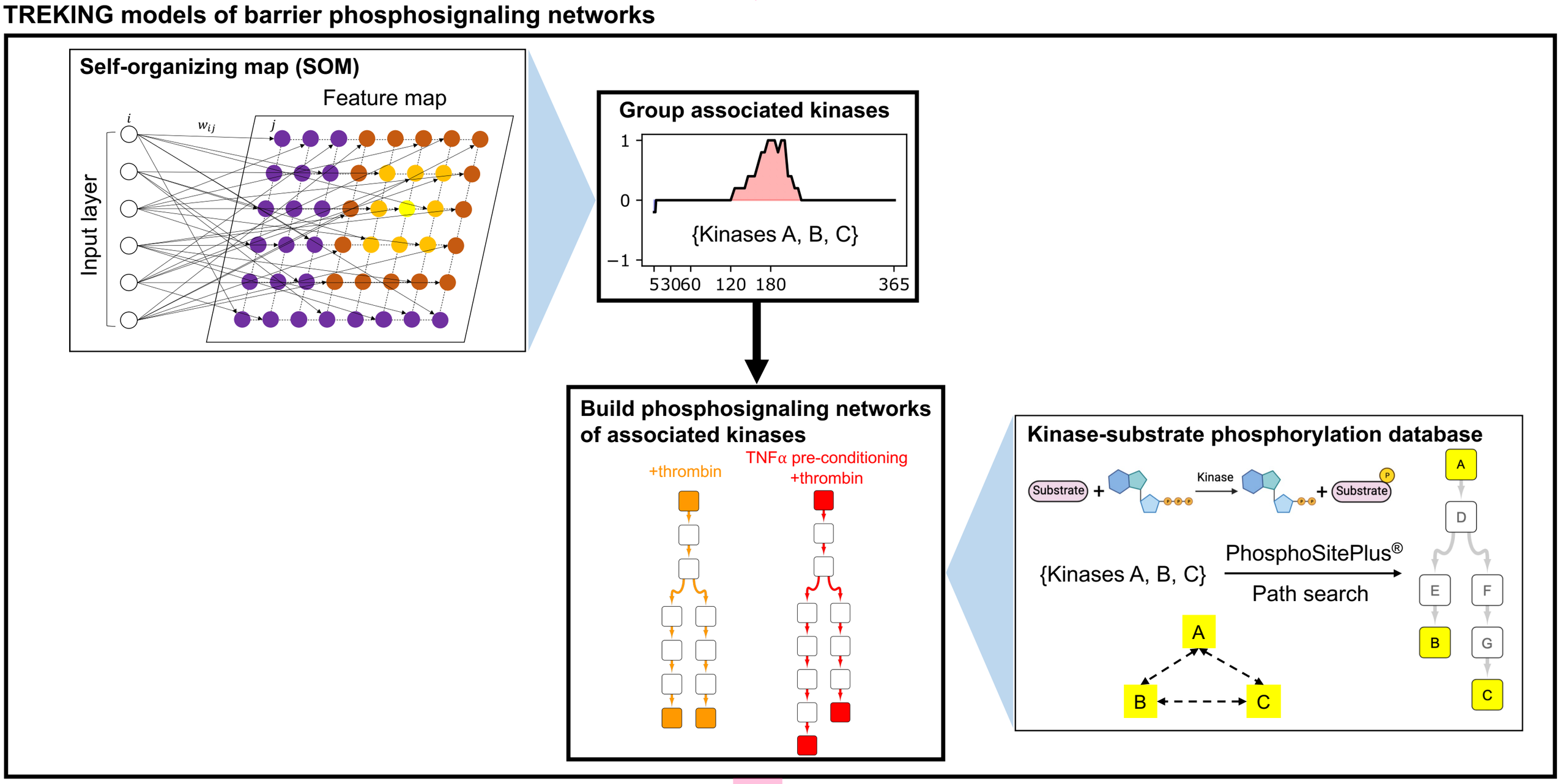

Comparison of western blot, tKiR functionality, and TREKING barrier phosphosignaling networks

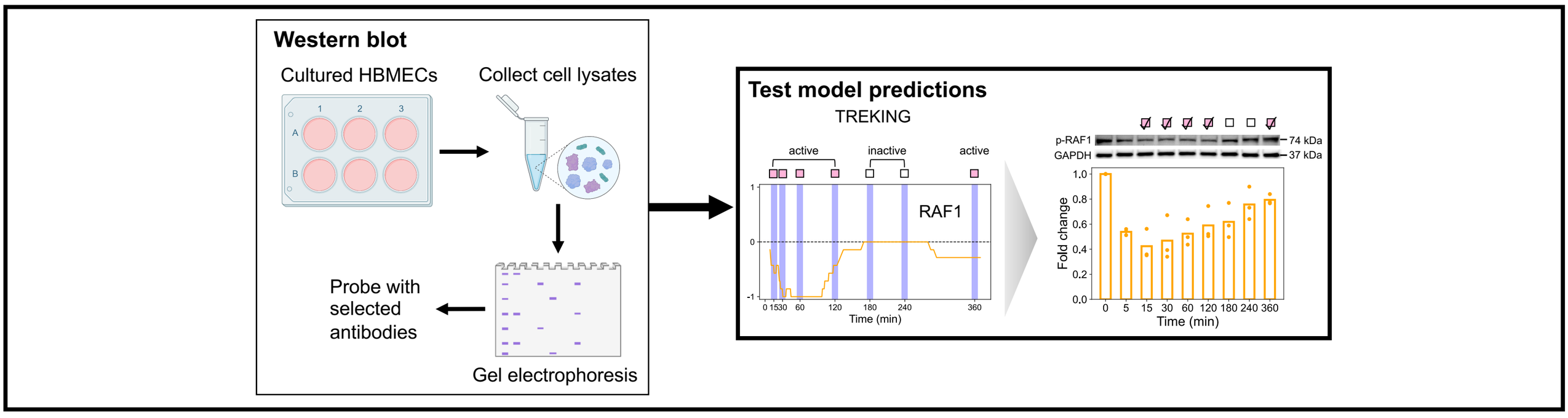

Figure S1

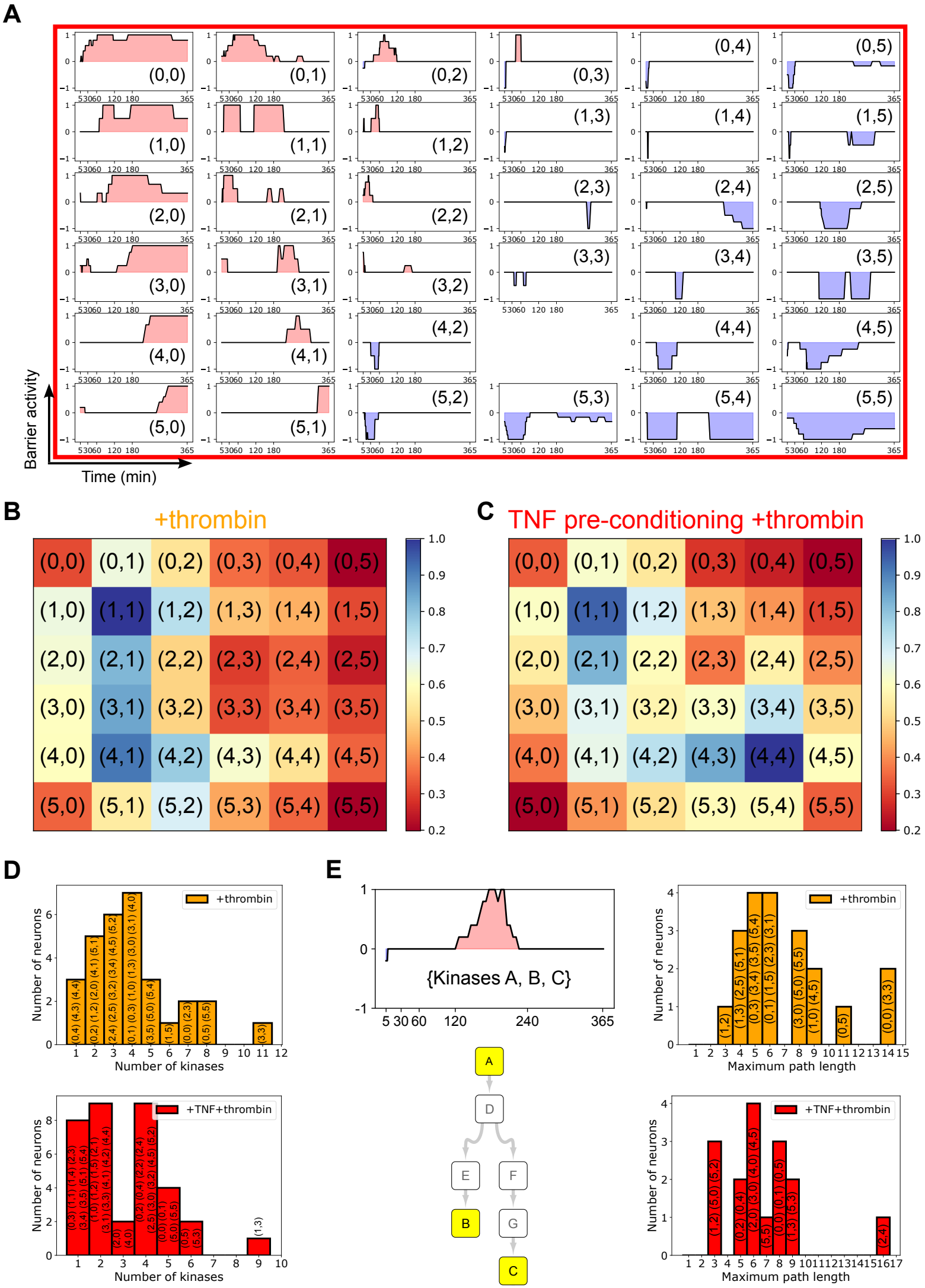
A
Barrier activity
Time (min)
B
+thrombin
C
TNF pre-conditioning +thrombin
D
+thrombin
Number of neurons
Number of kinases
+TNF+thrombin
Maximum path length
E
{Kinases A, B, C}
A
D
E
F
B
G
C

Figure S2

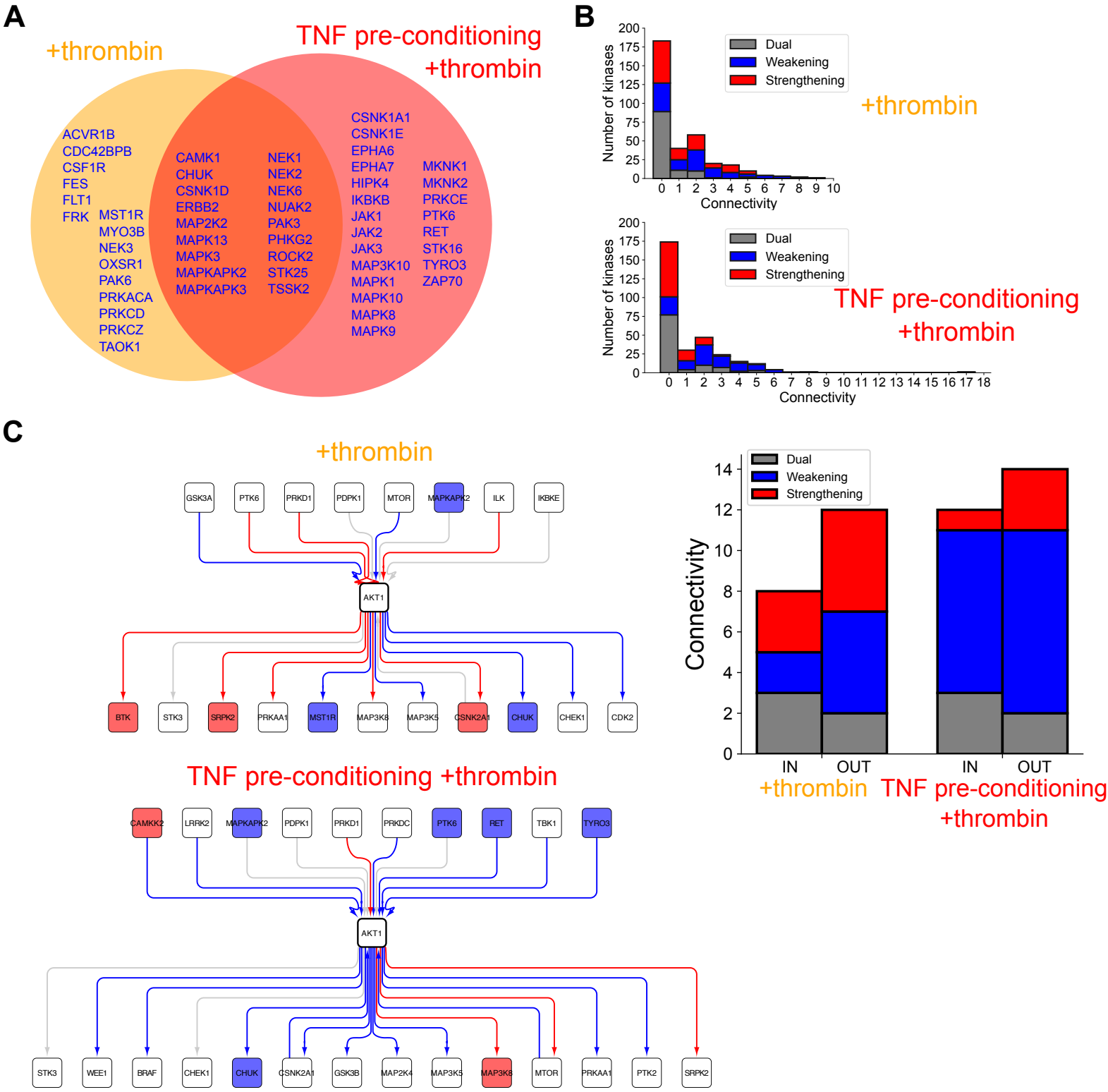
A
+thrombin
TNF pre-conditioning
+thrombin
ACVR1B
CDC42BPB
CSF1R
FES
FLT1
FRK
MST1R
MYO3B
NEK3
OXSR1
PAK6
PRKACA
PRKCD
PRKCZ
TAOK1
CAMK1
CHUK
CSNK1D
ERBB2
MAP2K2
MAPK13
MAPK3
MAPKAPK2
MAPKAPK3
NEK1
NEK2
NEK6
NUAK2
PAK3
PHKG2
ROCK2
STK25
TSSK2
CSNK1A1
CSNK1E
EPHA6
EPHA7
HIPK4
IKBKB
JAK1
JAK2
JAK3
MAP3K10
MAPK1
MAPK10
MAPK8
MAPK9
MKNK1
MKNK2
PRKCE
PTK6
RET
STK16
TYRO3
ZAP70
B
Number of kinases
Connectivity
Dual
Weakening
Strengthening
+thrombin
TNF pre-conditioning
+thrombin
C
+thrombin
GSK3A
PTK6
PRKD1
PDPK1
MTOR
MAPKAPK2
ILK
IKBKE
AKT1
BTK
STK3
SRPK2
PRKAA1
MST1R
MAP3K8
MAP3K5
CSNK2A1
CHUK
CHEK1
CDK2
TNF pre-conditioning +thrombin
CAMKK2
LRRK2
MAPKAPK2
PDPK1
PRKD1
PRKDC
PTK6
RET
TBK1
TYRO3
AKT1
STK3
WEE1
BRAF
CHEK1
CHUK
CSNK2A1
GSK3B
MAP2K4
MAP3K5
MAP3K8
MTOR
PRKAA1
PTK2
SRPK2
Connectivity
Dual
Weakening
Strengthening
IN
OUT
IN
OUT
+thrombin
TNF pre-conditioning
+thrombin

Figure S3

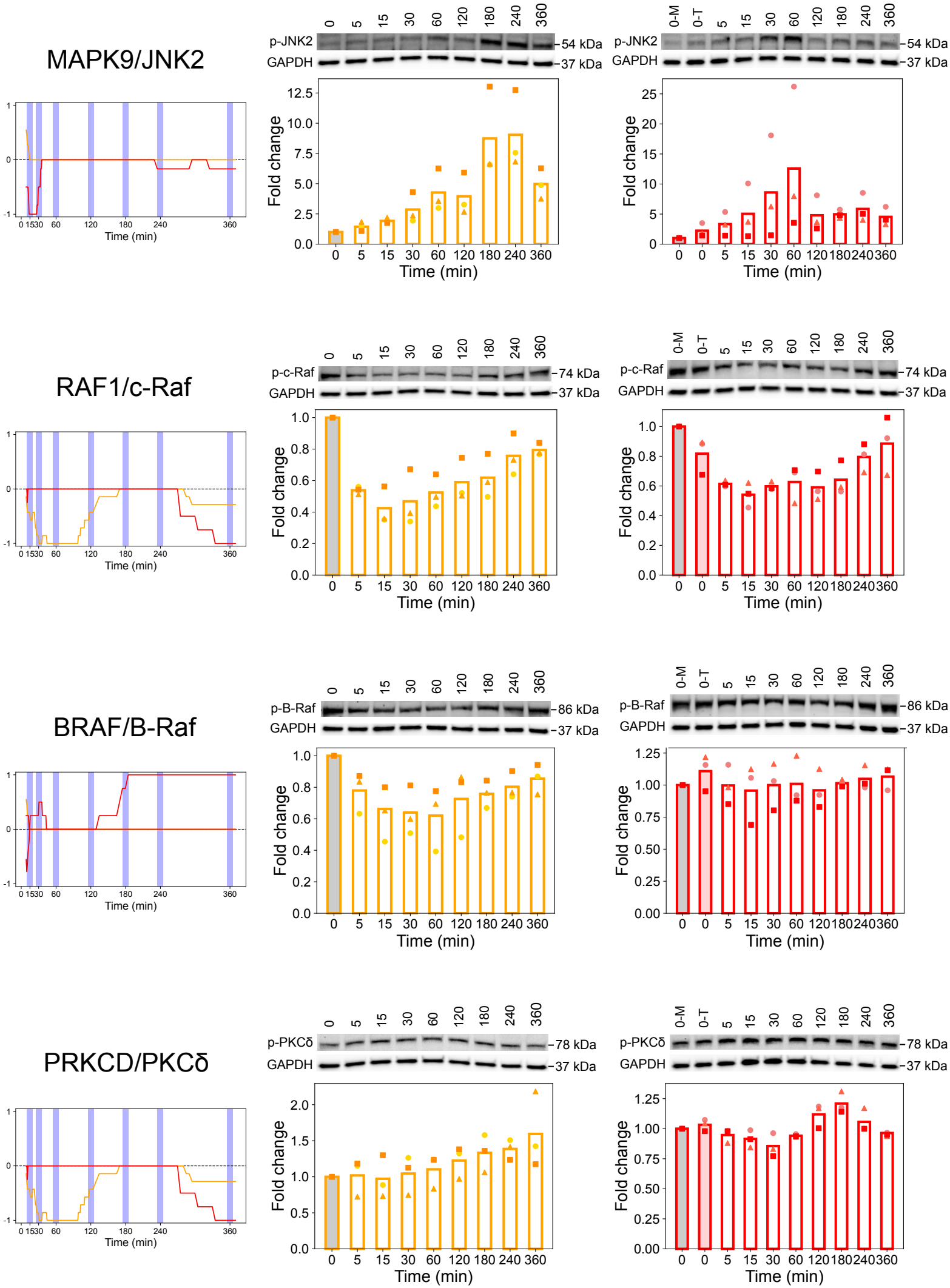
MAPK9/JNK2
p-JNK2
GAPDH
54 kDa
37 kDa
0-M
0-T
Fold change
Time (min)
RAF1/c-Raf
p-c-Raf
74 kDa
BRAF/B-Raf
p-B-Raf
86 kDa
PRKCD/PKCδ
p-PKCδ
78 kDa

Figure S4

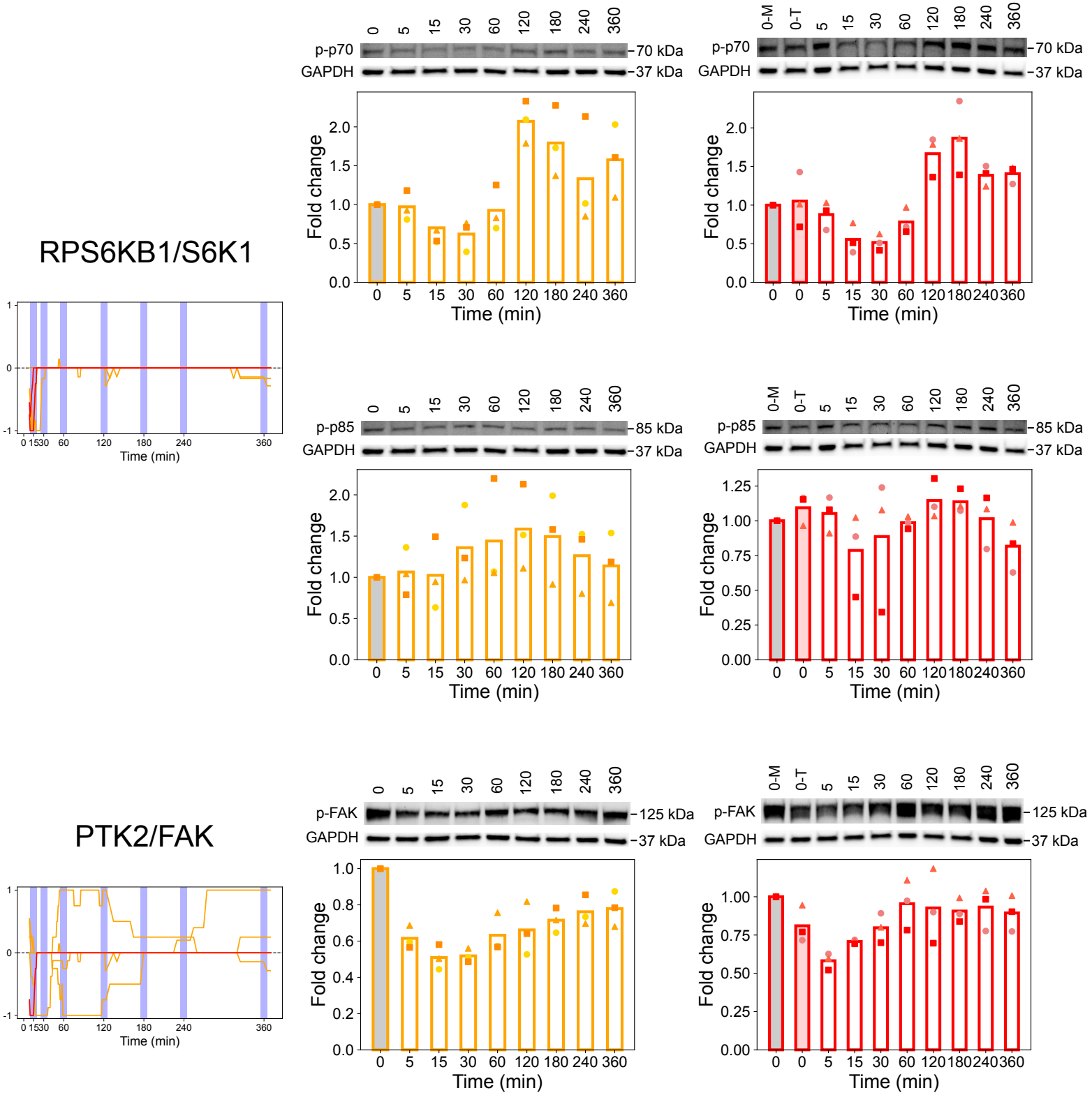
RPS6KB1/S6K1
PTK2/FAK
p-p70
GAPDH
70 kDa
37 kDa
p-p85
85 kDa
p-FAK
125 kDa
0-M
0-T
Fold change
Time (min)

Figure S4

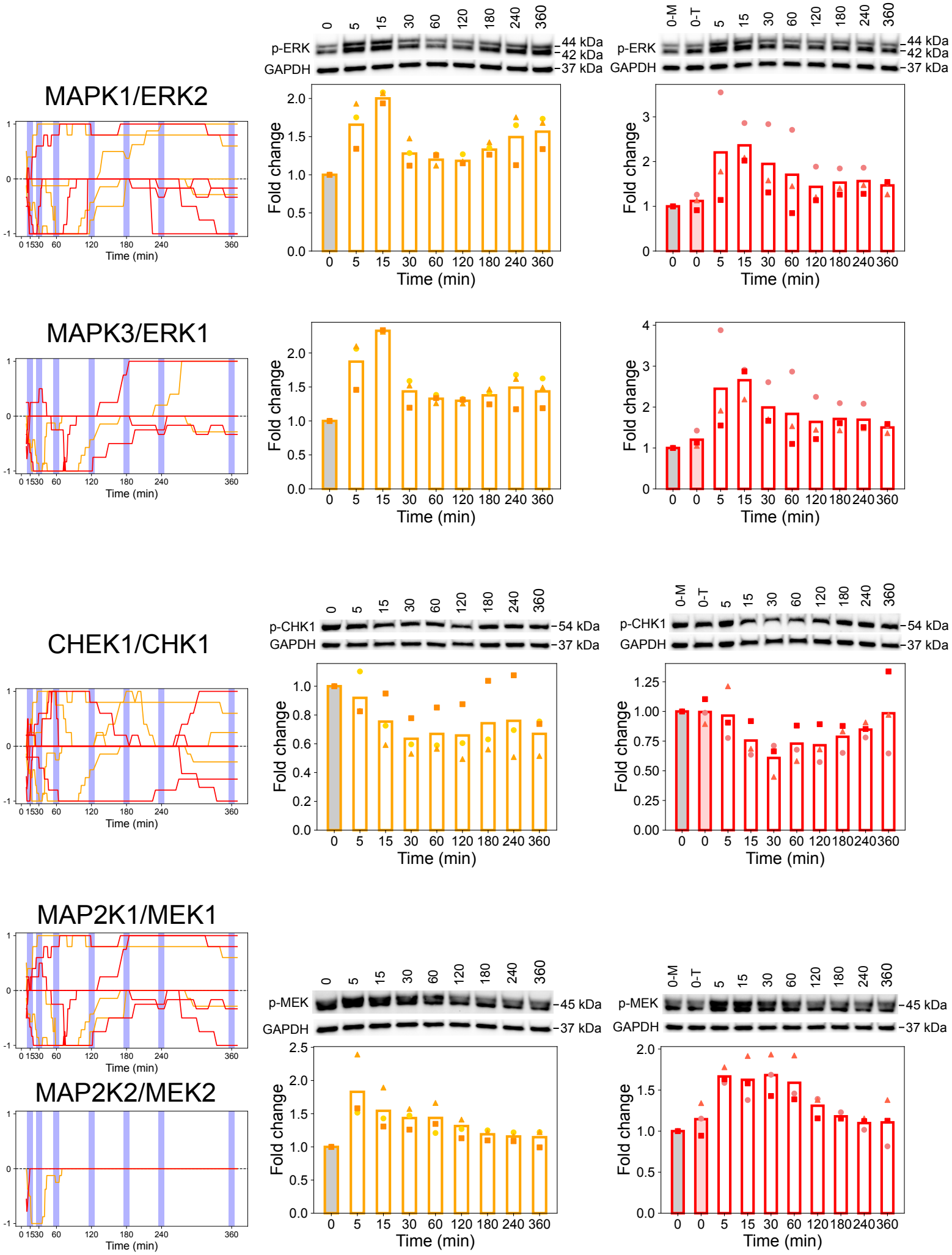
MAPK1/ERK2
p-ERK
GAPDH
44 kDa
42 kDa
37 kDa
0 5 15 30 60 120 180 240 360
0-M 0-T 5 15 30 60 120 180 240 360
Fold change
Time (min)
MAPK3/ERK1
CHEK1/CHK1
p-CHK1
54 kDa
MAP2K1/MEK1
p-MEK
45 kDa
MAP2K2/MEK2

Figure S4

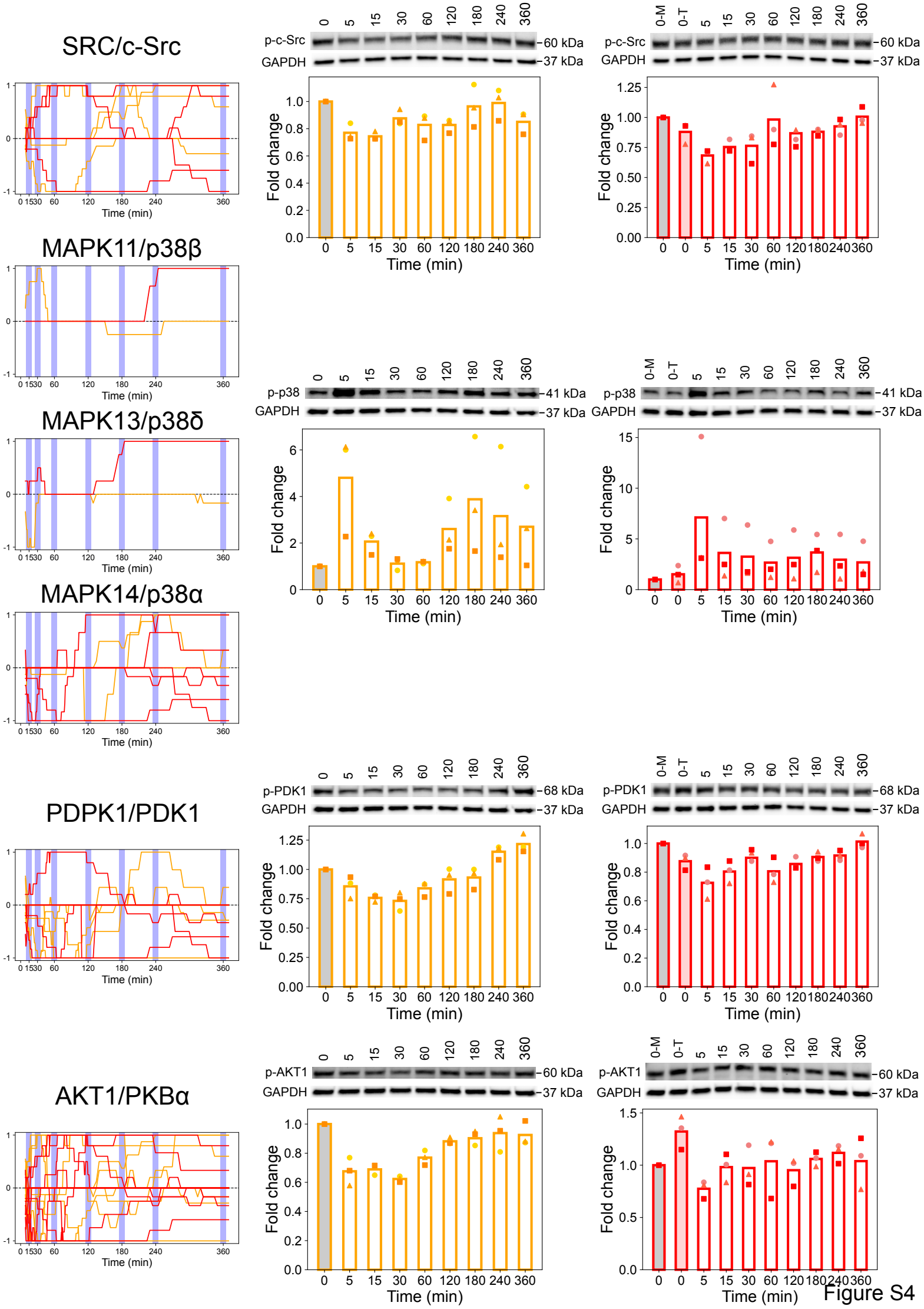
SRC/c-Src
MAPK11/p38β
MAPK13/p38δ
MAPK14/p38α
PDPK1/PDK1
AKT1/PKBα
p-c-Src
GAPDH
p-p38
p-PDK1
p-AKT1
60 kDa
37 kDa
41 kDa
68 kDa
0-M
0-T
Fold change
Time (min)

Figure S4

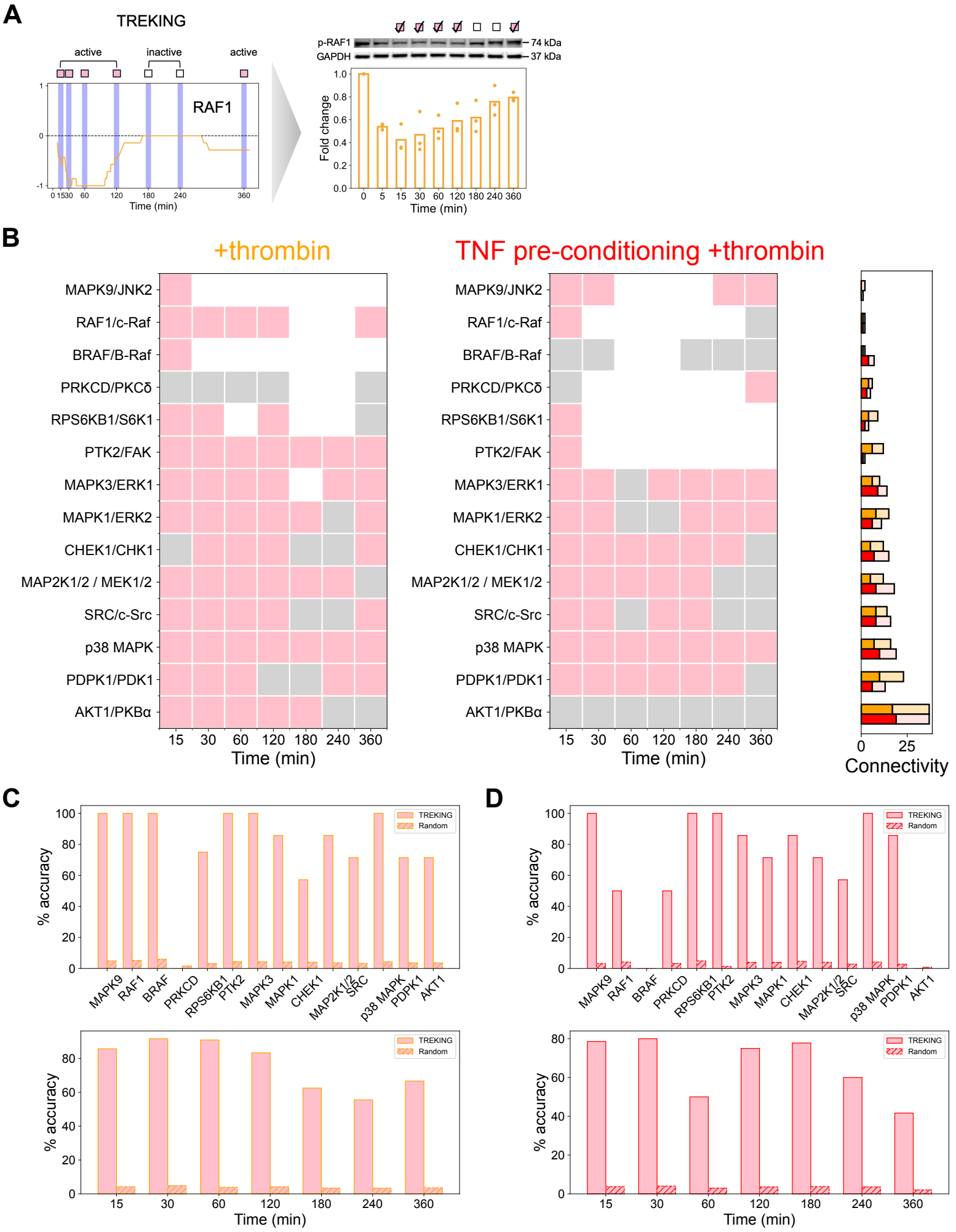
A
TREKING
active
inactive
active
RAF1
Time (min)
p-RAF1
GAPDH
74 kDa
37 kDa
Fold change
Time (min)
B
+thrombin
TNF pre-conditioning +thrombin
MAPK9/JNK2
RAF1/c-Raf
BRAF/B-Raf
PRKCD/PKCδ
RPS6KB1/S6K1
PTK2/FAK
MAPK3/ERK1
MAPK1/ERK2
CHEK1/CHK1
MAP2K1/2 / MEK1/2
SRC/c-Src
p38 MAPK
PDPK1/PDK1
AKT1/PKBα
Time (min)
Connectivity
C
D
% accuracy
TREKING
Random
MAPK9
RAF1
BRAF
PRKCD
RPS6KB1
PTK2
MAPK3
MAPK1
CHEK1
MAP2K1/2
SRC
p38 MAPK
PDPK1
AKT1
Time (min)

Figure S5

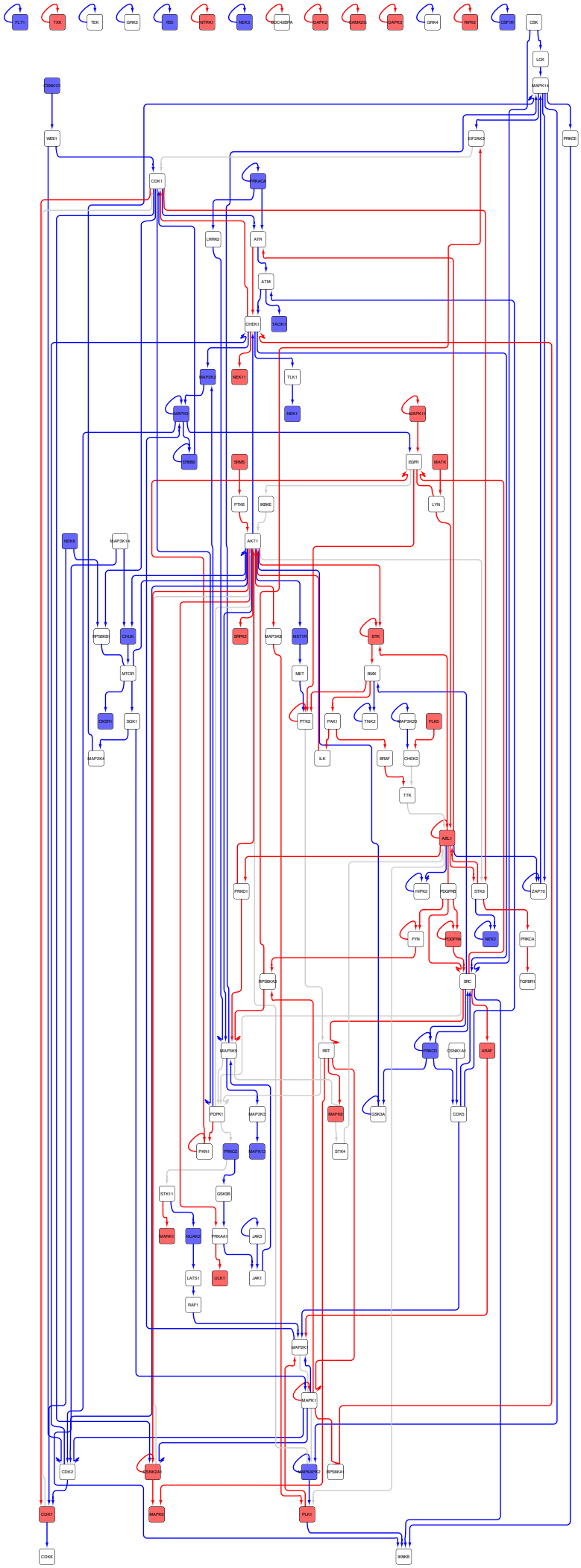
FLT1
TXK
TEK
GRK5
RIS
NTRK1
NEK3
DDC42BPA
DAPK2
CAMK2G
DAPK3
GRK4
RIPK2
CSF1R
CSK
LCK
MAPK14
CSNK1D
WEE1
EIF2AK2
PRKCE
CDK1
PRKACA
LRRK2
ATR
ATM
CHEK1
TACK1
MAP2K2
NEK11
TLK1
NEK1
MAPK3
MAPK11
EIF2B2
SRMS
EGFR
MATK
PTK6
IKBKE
LYN
NEK6
MAP3K14
AKT1
RPS6KB
CHUK
SRPK2
MAP3K8
MST1R
BTK
MTOR
MET
BMX
OKSR1
SGK1
PTK2
PAK1
TNK2
MAP3K20
PLK3
MAP2K4
ILK
BRAF
CHEK2
TTK
ABL1
PRKD1
HIPK2
PDGFRB
STK3
ZAP70
FYN
PDGFRA
NEK2
PRKCA
RPS6KA3
SFC
TGFBR1
MAP3K5
RET
PRKCD
CSNK1A1
ARAF
PDPK1
MAP2K3
MAPK8
GSK3A
CDK5
PKN1
PRKCZ
MAPK13
STK4
STK11
GSK3B
MARK1
NUAK2
PRKAA1
JAK3
LATS1
ULK1
JAK1
RAF1
MAP2K1
MAPK1
CDK2
CSNK2A1
MAPKAPK2
RPS6KA1
CDK7
MAPK9
PLK1
CDK6
IKBKB

Figure S6

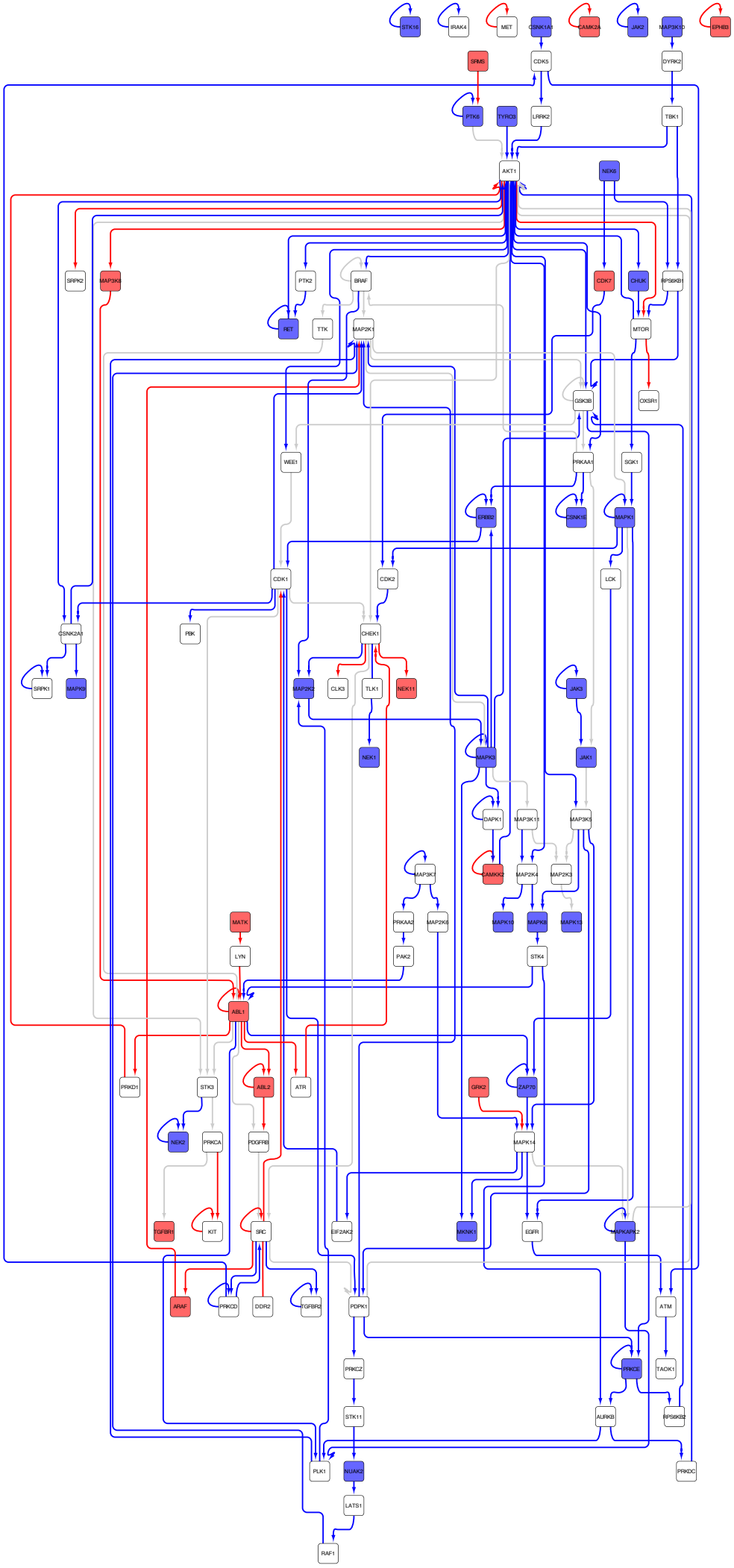
STK16
IRAK4
MET
CSNK1A1
CAMK2A
JAK2
MAP3K10
EPHB3
SRMS
CDK5
DYRK2
PTK6
TYRO3
LRRK2
TBK1
AKT1
NEK6
SRPK2
MAP3K6
PTK2
BRAF
CDK7
CHUK
RPS6KB1
RET
TTK
MAP2K1
MTOR
GSK3B
OXSR1
WEE1
PRKAA1
SGK1
ERBB2
CSNK1E
MAPK1
CDK1
CDK2
LCK
CSNK2A1
PBK
CHEK1
SRPK1
MAPK9
MAP2K2
CLK3
TLK1
NEK11
JAK3
NEK1
MAPK3
JAK1
DAPK1
MAP3K11
MAP3K5
MAP3K7
CAMKK2
MAP2K4
MAP2K3
MATK
PRKAA2
MAP2K6
MAPK10
MAPK8
MAPK13
LYN
PAK2
STK4
ABL1
PRKD1
STK3
ABL2
ATR
GRK2
ZAP70
NEK2
PRKCA
PDGFRB
MAPK14
TGFBR1
KIT
SRC
EIF2AK2
MKNK1
EGFR
MAPKAPK2
ARAF
PRKCD
DDR2
TGFBR2
PDPK1
ATM
PRKCZ
PRKCE
TACK1
STK11
AURKB
RPS6KB2
PLK1
NUAK2
PRKDC
LATS1
RAF1

Figure S7

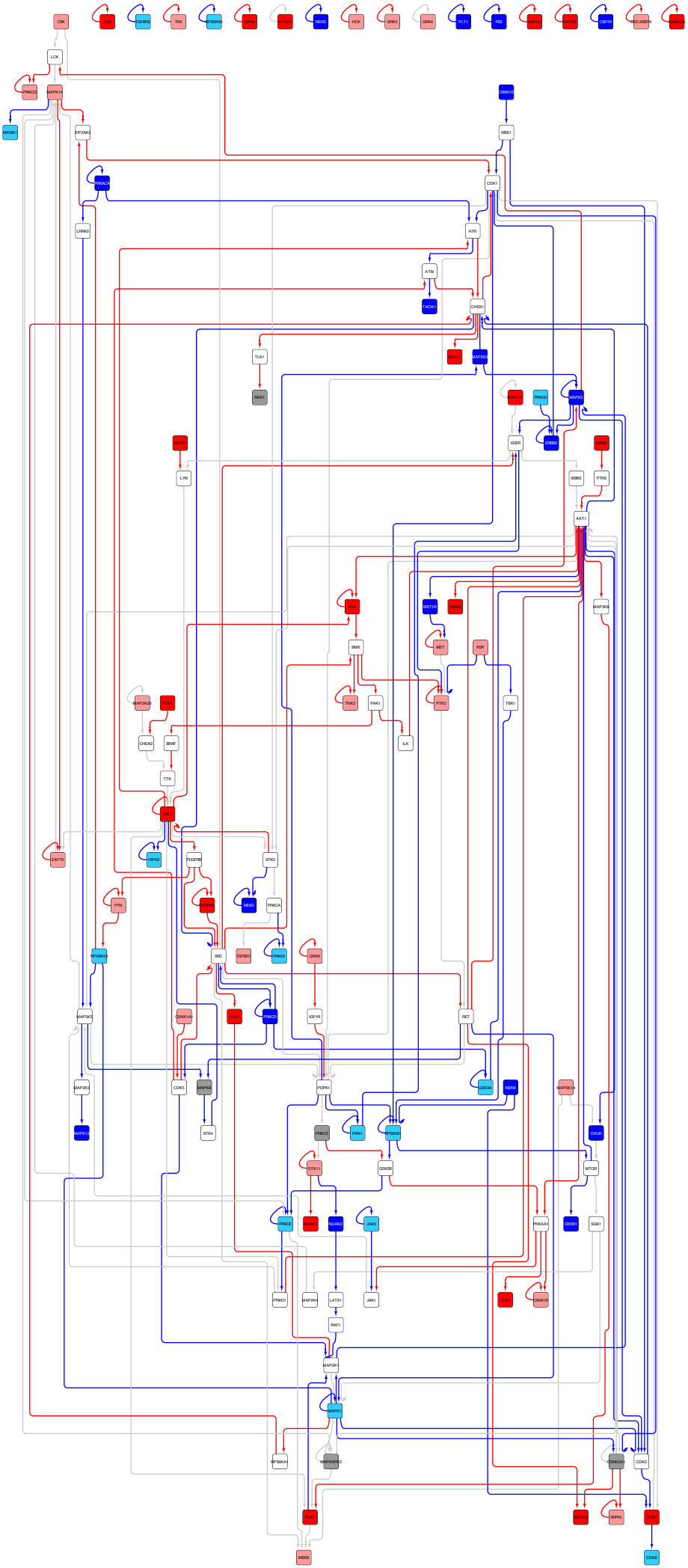

Figure S8

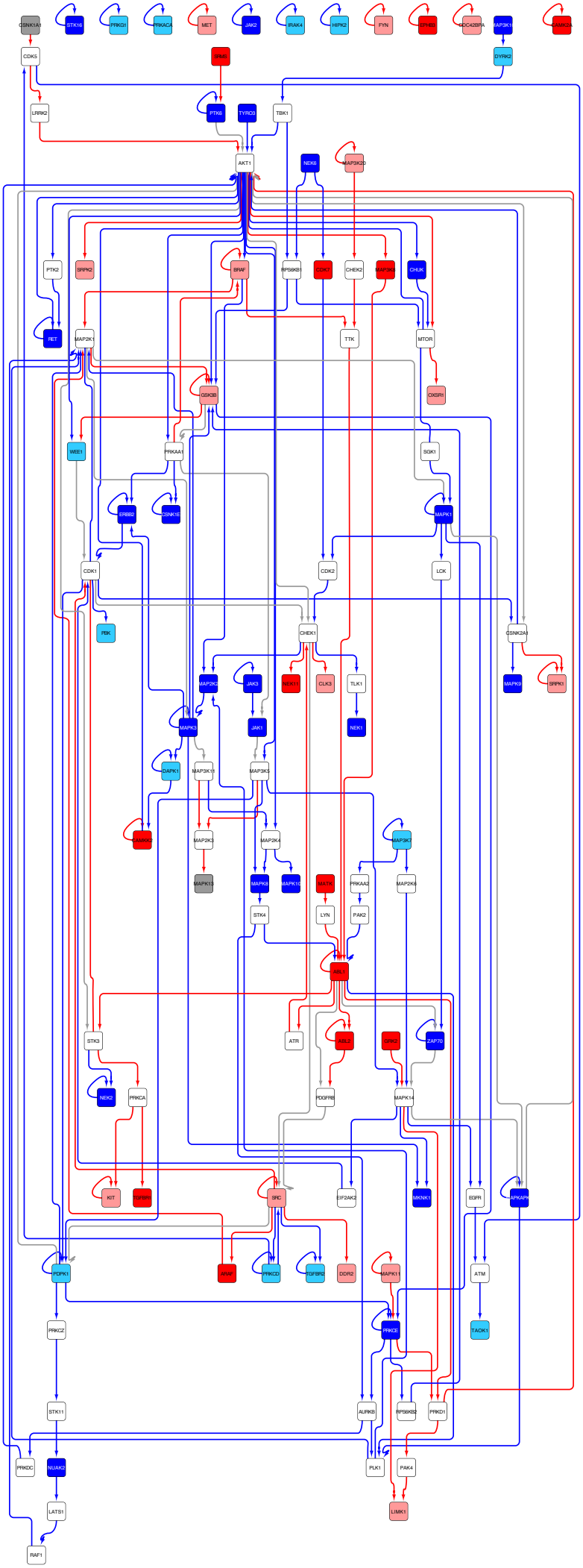
CSNK1A1
STK16
PRKG1
PRKACA
MET
JAK2
IRAK4
HIPK2
FYN
EPHB3
GOC42BPA
MAP3K1
CAMK2A
CDK5
SRM3
DYRK2
LRRK2
PTK6
TYRO3
TBK1
AKT1
NEK6
MAP3K20
PTK2
SRPK2
BRAF
RPS6KB1
CDK7
CHEK2
MAP3K8
CHUK
RET
MAP2K1
TTK
MTOR
GSK3B
OXSR1
WEE1
PRKAA1
SGK1
ERBB2
CSNK1E
MAPK1
CDK1
CDK2
LCK
PBK
CHEK1
CSNK2A1
MAP2K2
JAK3
NEK11
CLK3
TLK1
MAPK9
SRPK1
MAPK3
JAK1
NEK1
DAPK1
MAP3K11
MAP3K5
AMKK2
MAP2K3
MAP2K4
MAP3K7
MAPK13
MAPK8
MAPK10
MATK
PRKAA2
MAP2K6
STK4
LYN
PAK2
ABL1
STK3
ATR
ABL2
GRK2
ZAP70
NEK2
PRKCA
PDGFRB
MAPK14
KIT
TGFBR1
SRC
EIF2AK2
MKNK1
EGFR
APKAP4
PDPK1
ARAF
PRKCD
TGFBR2
DDR2
MAPK11
ATM
PRKCZ
PRKCE
TAOK1
STK11
AURKB
RPS6KB2
PRKD1
PRKDC
NUAK2
PLK1
PAK4
LATS1
LIMK1
RAF1

Figure S9